Appl. Phys. A 30, 1–22 (1983)

Applied Physics A Solids and Surfaces

Transition Metals in Silicon

Eicke R. Weber

Abteilung für Metallphysik, II. Physikalisches Institut, Universität zu Köln, D-5000 Köln 41, Fed. Rep. Germany

Received 19 August 1982/Accepted 5 October 1982

Abstract. A review is given on the diffusion, solubility and electrical activity of 3*d* transition metals in silicon. Transition elements (especially, Cr, Mn, Fe, Co, Ni, and Cu) diffuse interstitially and stay in the interstitial site in thermal equilibrium at the diffusion temperature. The parameters of the liquidus curves are identical for the Si:Ti – Si:Ni melts, indicating comparable silicon-metal interaction for all these elements. Only Cr, Mn, and Fe could be identified in undisturbed interstitial sites after quenching, the others precipitated or formed complexes. The 3*d* elements can be divided into two groups according to the respective enthalpy of formation of the solid solution. The distinction can arise from different charge states of these impurities at the diffusion temperature. For the interstitial 3*d* atoms remaining after quenching, reliable energy levels are established from the literature and compared with recent calculations.

PACS: 61.70 Wp, 71.55 Fr, 82.60 s

The first systematic study of properties of transition metals in silicon has been performed in the early sixties by Ludwig and Woodbury. Their papers on Electron Paramagnetic Resonance (EPR) investigations of transition metal doped silicon [1,2] up to now are a source of valuable information in this field.

Diffusion and solubility data of impurities in silicon have been compiled by Trumbore in 1960 [3]. These values are used till today, see, e.g., [4], although they are partly out of date because of the lower level of semiconductor technology at that time.

The situation is even worse regarding electrical properties of transition metals in silicon. Generally their importance as fast diffusers during any heat treatment of silicon devices has been recognized. However, experiments with rather unspecific methods like resisitivity or Hall effect measurements, the use of poorly defined specimens, contamination during diffusion treatment and uncontrolled complexing reactions resulted in a tremendous amount of data that can hardly be ascribed to specific defects and defect configurations. Electrical data, as reviewed recently [5], have thus to be treated with care. In most cases the defect configuration is not reliably established. As an example, Graff and Pieper [6] demonstrated that the energy levels quoted for iron in silicon cover the whole band gap. The same holds for most of the other transition elements.

This paper aims to describe properties of 3*d* transition metal ions in silicon (especially, Cr, Mn, Fe, Co, Ni, and Cu) clearly related with well defined defect configurations. New diffusion and solubility results have been derived by a combination of EPR measurements with Neutron Activation Analysis (NAA) [7–11].

As a result the dominance of interstitial diffusion and solution at high temperatures in thermal equilibrium is deduced for all these elements. Yet only Cr, Mn, and Fe can be quenched into interstitial sites: Co, Ni, and Cu precipitate already during cooling. Interstitial 3*d* metals are still mobile at room temperature, forming complexes with shallow acceptors, if present. Energy-level determinations of 3*d* metals in Si are critically discussed in the last paragraph as far as these results can be related with specific 3*d* metal species.

0721-7250/83/0030/0001/$04.40

This work shows that 3*d* transition elements in silicon behave similarly, revealing clear trends with respect to their position in the periodic table. Thus a foundation may be given for further realistic theoretical work in this field the advent of which just is noticeable [12–15].

1. Experimental Methods

Experimental methods generally used for diffusion and solubility studies of semiconductors have been described in various publications, see, e.g., [16, 17]. Here mainly procedures used for the combined EPR and NAA investigations [7–11] are treated in detail.

1.1. Diffusion Treatment

For those investigations [7–11] samples of dislocation-free floating-zone silicon (Wacker Chemitronic) of typically $4 \times 4 \times 15\,mm^3$ were used. Shallow doping was $10^{13}\,B/cm^3$ ("*i*-Si") and up to $5 \times 10^{16}\,B/cm^3$ or P/cm^3. After mechanically and chemically polishing they were plated with the transition metal in vacuum ($10^{-3}\,Pa$) onto the four side faces. Diffusions were performed in a vertical SiC tube furnace, the samples being in a quartz tube flushed by reducing gas (8% H_2, 92% N_2) [7]. Temperatures were stabilized within $\pm 0.5\,K$. Samples with different diffusion times were prepared at each temperature to ensure homogenous distribution. Thus each solubility determination in [8–11] represents several (up to ten) concentration determinations. After diffusion the specimens were quenched in diffusion pump oil achieving a cooling rate of about 500 K/s. Next, a surface layer of at least 100 μm was mechanically and chemically removed. The samples were stored at 77 K prior to EPR work.

1.2. EPR *Spectroscopy*

For EPR measurements a Bruker BER 420 spectrometer working in the X-band was used. By means of a helium gas flow cryostat sample temperatures between 6 K and 300 K could be stabilized. Concentrations of paramagnetic species were determined by comparison of spectra measured in slow passage conditions. As standards a calibrated NBS $Al_2O_3:Cr^{3+}$ probe [18] and the EPR spectrum of P_s^0 in *n*-Si crystals of various doping levels were used (subscript s: substitutional, i: interstitial). The magnitude of Cr_i^+ spectra in *p*-Si with $[B_s] < [Cr_i]$ is proportional to the boron content, allowing an additional calibration for Cr_i^+ concentrations. All three methods resulted in coinciding concentration values within an error margin of 30%. This can be considered as a realistic estimation of the total error in spin concentration determinations by EPR.

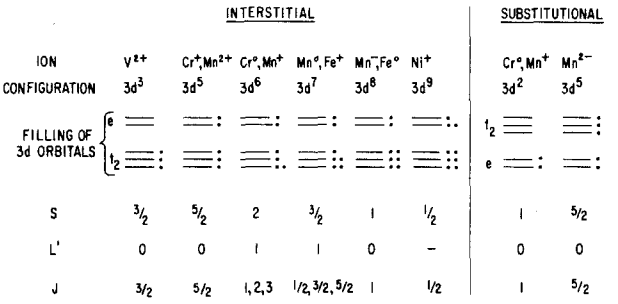

Fig. 1. Electronic structure of 3*d* metal ions in silicon, according to Ludwig and Woodbury [1]. The symbols *S*, *L'*, and *J* represent total spin, effective orbital angular momentum, and effective total angular momentum, respectively

Most EPR spectra of transition metal doped silicon have been described by Ludwig and Woodbury [1, 2]. They developed a model for the electron states of interstitial and substitutional 3*d* metals in silicon (Fig. 1) which successfully explains the observed EPR spectra. The basic assumption of this model is promotion of the 4*s* electrons into the 3*d* shell for a 3*d* metal in silicon. On *interstitial* sites (of tetrahedral symmetry) the 3*d* states are split into a triplet t_2 and a doublet *e*, each of which has, in addition, twofold spin degeneracy. The strongly localized covalent bonding of the surrounding silicon atoms concentrates valence electron density between the host atoms. The interstitial experiences thus a cubic crystal field arising from not completely shielded nuclear positive charges [19]. The result is lowering the energy of t_2 states with respect to the *e* doublett. *Substitutional* 3*d* metal atoms could never be found after quenching, cf. [20]. They could be produced out of interstitial species by trapping of (e. g., irradiation induced) vacancies [1]. The Ludwig and Woodbury model assumes formation of covalent bonds with the silicon neighbours by hybridization of four of the 3*d* electrons. The substitutional atom is in an effective cubic crystal field of negative charges from the surrounding valence electrons so that for the remaining 3*d* electrons the *e* states are lower in energy than the t_2 states. The crystal field splitting between t_2 and *e* must be small as the observed spectra show filling of these states according to Hund's rule with maximum spin. The Ludwig and Woodbury model not only described correctly the effective numbers of electrons and resulting spins of 3*d* elements in silicon in various charge states (Fig. 1), but as well the *g*-values and temperature dependences of the spectra, [1, 2].
Solubility investigations by EPR of Cr, Mn, and Fe diffused and quenched Si samples [8–11] provided spectra of interstitial ions on sites with tetrahedral symmetry and metal-acceptor pairs. The resonance parameters were in accordance with [1, 2]. Solubility determinations resulting from these experiments are

discussed in Sect. 3. In the following, qualitative features of the observed spectra are considered briefly for each element.

Iron was measured in *i*-Si and *n*-type silicon as Fe_i^0 [8]. In *p*-Si, in addition, Fe_i^+ appeared at the expense of Fe_i^0. Therefore a donor level and no acceptor action of Fe_i can be expected. In *p*-type samples pairing of interstitial Fe with substitutional B took place during room temperature storage (Sect. 2.3), resulting in the EPR spectrum of $(Fe_i^+B_s^-)^0$. This spectrum vanished for small compensation ($[Fe_i]<[B]$) when only Fe_i^+ was measurable and the Fermi energy was close to the boron acceptor level. In this case, illumination with band-gap light leads to appearence of both spectra, Fe_i^0 and $(FeB)^0$. Using higher Fe concentrations, $(FeB)^0$ and Fe_i^+ can be measured simultaneously, so that the corresponding energy levels appear to be in the following order:

$$E_v<(B_s)^{-/0}<(FeB)^{0/+}<(Fe_i)^{0/+} \quad (1)$$

with E_v the valence band edge, $(B_s)^{-/0}$ the acceptor level of substitutional B (B_s^-/B_s^0), $(FeB)^{0/+}$ the donor level of (FeB) pairs, and $(Fe_i)^{0/+}$ the donor level of interstitial iron.

Interstitial *manganese* was observed in the charge states Mn_i^0 and Mn_i^- depending on the kind and level of shallow doping. EPR solubility values [10, 11] were obtained from Mn_i^0 concentrations determined in *i*-Si samples. Samples quenched less rapidly out of a horizontal furnace showed weaker or no Mn_i spectra but the characteristic 21 line pattern of 4 tetrahedrally clustered Mn atoms [21] indicating clustering during cooling down. In addition, even most rapid quenching from temperatures above 1150 °C did not produce Mn_i concentrations markedly higher than from 1100 °C so that in this case, too, clustering and precipitation of part of this high Mn content takes place.

The resonance of *chromium* as Cr_i^0 is observable only at low temperatures ($T<6$ K) because of strong line broadening [22] of this non *S*-state ion (Fig. 1). Thus Cr_i concentrations were derived from measurements of Cr_i^+ [9–11]. The concentration $[Cr_i^+]$, being proportional to $[B_s]$ as long as $[B_s]<[Cr_i]$, gets independent of $[B_s]$ for $[B_s]>[Cr_i]$. For $B_s \lesssim 10^{15}/cm^3$, $(CrB)^0$ pair spectra [1] appeared after room temperature storage, accompanied by a reduction of the Cr_i^+ signal. The EPR observations give no support for the existence of a stable Cr_i^{++} charge state discussed in the literature, [1, 23]. Those conclusions concerning the Cr_i^{++} state might have been influenced by insufficiently controlled complexing reactions, especially CrB pair formation. The paramagnetic $(CrB)^0$ charge state had in most cases (with $[B_s]>[Cr_i]$) to be produced by band gap illumination, indicating the existence of a donor level $(CrB)^{0/+}$.

In *cobalt* doped silicon only EPR signals of Fe contaminations could be detected (in the $10^{13}\,cm^{-3}$ concentration range) though NAA confirmed the presence of Co in the diffused samples [9–11]. Cobalt present in thermal equilibrium at high temperatures as interstitial cannot be kept in these sites during quenching due to its high diffusivity (Sect. 2.2). It forms rather complexes or precipitates as observed by Mössbauer spectroscopy [24]. Similarly in *copper* doped silicon no Cu – related EPR signal was found.

P-type *nickel* doped samples showed a weak signal at $g=2.026$ corresponding to concentrations of $10^{13}-10^{14}\,cm^{-3}$ independent of diffusion temperature. This spectrum has been ascribed by Ludwig and Woodbury [1] to interstitial Ni_i^+. Interstitial Ni is as mobile as Cu_i or Co_i (Fig. 2). Consequently, it is as unstable as those elements during quenching and room temperature storage. Therefore this EPR spectrum originates probably from a Ni_i ion stabilized by some additional defect. Such an interpretation is in accordance with the EPR data showing this ion to be in a distorted site [1].

In addition, a new EPR spectrum [25] was detected in Ni doped, quenched *i*-Si, labelled Si-K 9, with $S=1/2$ and an anisotropic *g*-tensor with ⟨111⟩-axis of symmetry. It occured in concentrations near $5\times10^{13}\,cm^{-3}$. The *g*-values are:

$$g_{\parallel}=2.0008\pm0.0003$$

$$g_{\perp}=2.0086\pm0.0003.$$

This *g*-tensor is almost identical with the "Si-B 4" spectrum found in electron irradiated and subsequently at 275 °C annealed silicon [26]. It is similar to many EPR spectra ascribed to vacancy – type point defect clusters containing an unpaired dangling bond at a Si atom [27, 28].

Ludwig and Woodbury [1] observed the change of interstitial 3*d* atoms, e.g. Mn_i, to substitutional sites not only by irradiation as mentioned above but as well during cooling of a supersaturated T-metal solution (e.g. Cu, codiffused with Mn). The explanation for this change was vacancy emission out of stress fields around precipitating copper. These vacancies were thought to be trapped by interstitial Mn atoms converting them to substitutional sites. Obviously the Si-K 9 centers confirm for the first time directly the presence of these precipitation induced vacancy clusters for Si:Ni.

1.3. Neutron Activation Analysis

Total concentrations of 3*d* metals in diffused silicon samples were established by means of NAA [7–11, 29]. For background reduction during γ-counting an Anticompton spectrometer working as anticoinci-

Table 1. Diffusion coefficients in silicon

Diffusant	Diffusion coefficient D [cm^2/s]	Temperature range [°C]	D (1100 °C) [cm^2/s]	Method	Estimated values of D [cm^2/s][a]	Ref.
Ti	$2 \times 10^{-5} \exp(-1.5\,[eV]/kT)$	1000–1250	6×10^{-11}	Tracer		[35][b]
V	$\sim 10^{-7}$	900–1100	$\sim 10^{-7}$	DLTS		[36]
Cr	$10^{-2} \exp(-1.0\,[eV]/kT)$	900–1250	2×10^{-6}	p/n jct.		[37][c]
			$\sim 10^{-6}$	NAA	900 °C: 4×10^{-7}	[11]
Mn	10^{-6}–2×10^{-5}	1000–1350	$\sim 3 \times 10^{-6}$	Tracer		[38]
			$\sim 2 \times 10^{-6}$	NAA	1100 °C: 2×10^{-6}	[11]
Fe	$6.2 \times 10^{-3} \exp(-0.87\,[eV]/kT)$	1100–1250	4×10^{-6}	Tracer		[39]
	$4 \exp(-0.9\,[eV]/kT)$	~ 20		DLTS		[40]
	$1.3 \times 10^{-3} \exp(-0.68\,[eV]/kT)$	20–1250	4×10^{-6}	Various	1100 °C: 4×10^{-6}	[11][d]
Co	10^{-6}–10^{-4}	1000–1300	$\sim 10^{-5}$	Tracer		[41]
			$> 10^{-5}$	NAA	700 °C: $> 7 \times 10^{-6}$	[11][e]
Ni	$2 \times 10^{-3} \exp(-0.47\,[eV]/kT)$	800–1300	4×10^{-5}	Tracer		[42]
			$> 10^{-5}$	NAA	700 °C: $> 10^{-5}$	[11][f]
Cu	$4.7 \times 10^{-3} \exp(-0.43\,[eV]/kT)$	400–900	1×10^{-4}	Tracer		[43]
			$> 10^{-5}$	NAA	500 °C: $> 10^{-5}$	[11]
Zn	10^{-7}–10^{-6}	1100–1300	$\sim 10^{-7}$	Tracer		[44]
Li	$2.5 \times 10^{-3} \exp(-0.66\,[eV]/kT)$	25–1350	1×10^{-5}	Various		[45][g]
B	$5.1 \exp(-3.70\,[eV]/kT)$		1×10^{-13}			[46][g,h]
P	$10.5 \exp(-3.69\,[eV]/kT)$	1050–1350	3×10^{-13}	p/n jct.		[47][g,h]
^{31}Si	$1460 \exp(-5.02\,[eV]/kT)$	1050–1385	5×10^{-16}	Tracer		[48][i]

[a] Estimated values have been derived from NAA measurements [8–11] of the time necessary for 50% saturation of metal-plated samples. The error margin of such an estimation is a factor of 2

[b] The Si:Ti diffusion data of Boldyrev et al. [35] clearly need further confirmation

[c] Bendik et al. [37] additionally observed by EPR annealing of Cr_i^+ near 200 °C with an activation energy of 0.91 eV in accordance with the high-temperature activation energy

[d] Common fit of all Si:Fe diffusion data (Fig. 4)

[e] Further Co diffusion data [49] with surprisingly high activation energy of 2.8 eV have been ascribed to uncoltrolled outdiffusion during cooling down [24]

[f] Ni diffusion results of Bonzel [50] are omitted as they are obtained based on the erroneous assumption of dissociative diffusion, cf. e.g. Hu [34]. The values given are in accordance with further estimations [51, 52]

[g] Further data can be found e.g. in [34] and [53]

[h] A re-interpretation of group III and V diffusion results in favour of the self-interstitial model is discussed by Gösele et al. [54]

[i] For discussions of possible models of self-diffusion in silicon [53–57]

dence shield was employed, thus achieving lowest detection limits for instrumental NAA of Si [10, 29].

1.4. Electrical Measurements

Energy level determinations of 3*d* elements in silicon using electrical methods are critically reviewed in Sect. 4. Here a short description of some relevant experimental techniques is given.

In recent years *junction techniques* are more and more preferred rather than Hall effect measurements used predominantly in the past for energy level determinations in semiconductors. These junction techniques are defect-specific as they offer the possibility to determine the concentration and energy levels of deep level defects even when several kinds of defects are present in one sample. An example for non-transient junction techniques are thermally stimulated capacitance change measurements [30] (TSCAP or TSCA). In such an experiment the thermal release of carriers out of deep levels in a reverse biased p/n junction is monitored during warming up of the sample.

Transient junction techniques like Deep Level Transient Spectroscopy (DLTS) [31] are more sensitive. These techniques measure the thermally stimulated change of capacitance or current transients after a carrier pulse. Besides measurement of energy levels and defect concentrations ($\gtrsim 10^9\,cm^{-3}$) these transient techniques allow determination of capture cross sections and further properties of deep levels in the depletion region of a p/n or Schottky junction. Reviews on junction transient techniques have been given e.g. by Miller et al. [32] and Grimmeiss [33].

2. Diffusion of 3*d* Transition Metals in Silicon

2.1. Diffusion Coefficients in Silicon

Motion of atoms in a solid usually proceeds by thermally activated jumping over potential barriers between different sites. The diffusion constant can therefore be expressed as

$$D = D_0 \exp(-Q/kT) \quad (2)$$

with an activation energy Q related to the barrier height and a temperature independent preexponential D_0 which contains the attempt frequency for this process and the migration entropy, [34].

Transition metals are well known to be fast diffusers in silicon at high temperatures ($T > 0.7\,T_m$; T_m: melting temperature). Diffusion coefficients of T-metals and some other typical elements for comparison are given in Table 1 and Fig. 2. The diffusivity increases with increasing atomic number in the 3*d* row up to Ni and Cu with the largest diffusion coefficients known in silicon. Most diffusion coefficients are in the 10^{-5} cm^2/s range near the melting point. Such diffusivities are typical for solute atoms in liquids [58]. Concentrations of native defects like vacancies or self-interstitials in silicon are very low [56, 59, 60] so that these high diffusion coefficients can only be explained by an interstitial diffusion mechanism independent of native lattice defects. The activation energies Q for this interstitial diffusion of T-metals in silicon are found to be in the range 0.5–1.0 eV (Table 1).

In contrast to the T-metals, elements of the IIIrd and Vth group forming covalent bonds with the host atoms diffuse via substitutional mechanism as do Si atoms themselves. For these processes the activation energy Q consists of the energy of formation of a native defect (vacancy [55] or self-interstitial [56]) plus the energy of migration of the diffusant. Q is about 5 eV for ^{31}Si in Si [48] and 3.7 eV for P or B in Si [46, 47]. Typical substitutional diffusion coefficients even near the melting point are in the 10^{-11} cm^2/s range (Table 1 and Fig. 2).

The large preexponential factor of self-diffusion leads to the conclusion that an extended native defect with a high entropy of formation is involved. However, it is still debated whether this defect is of the vacancy type, e.g. [55, 61], or of the interstitial type as proposed by Seeger et al. [56, 57]. Several attempts have been made to deduce information on the nature of the dominant native defect out of diffusion and solubility studies of transition metals in Si [56, 57, 62, 63] so that this question will be treated further in the next subsection.

2.2. Interstitial Diffusion of 3d Metals

As a typical example for diffusion of 3*d* metals into silicon Fig. 3 shows the concentration of iron in Si vs

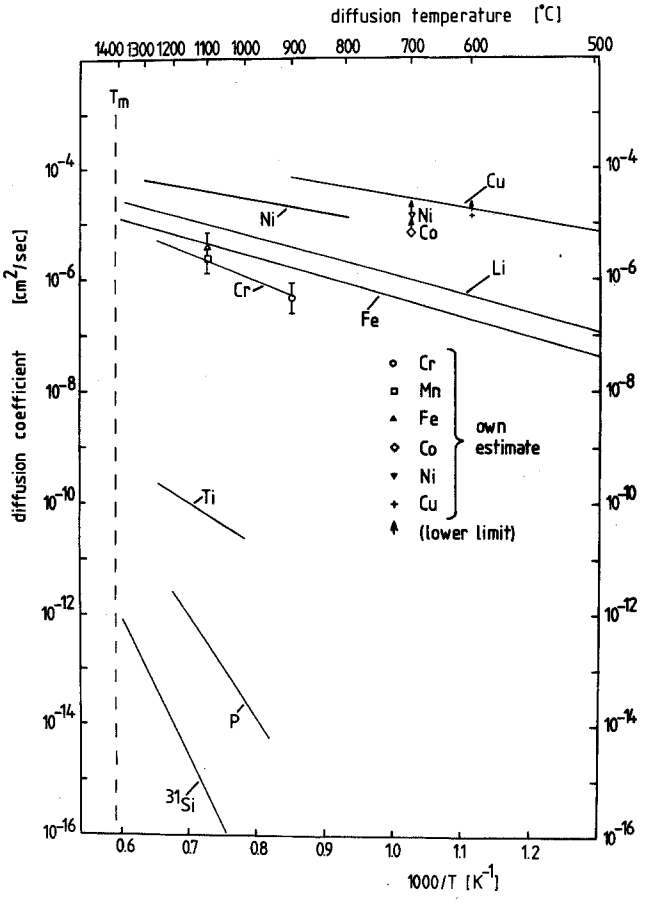

Fig. 2. Temperature dependence of diffusion coefficients of 3*d* metals and some substitutional diffusants in silicon. The corresponding references are given in Table 1. For Si:Fe the result of Fig. 4 is included, obtained from combination of various diffusivity results. Estimated values have been derived from the time necessary for 50% saturation of metal-plated NAA samples [8–11]

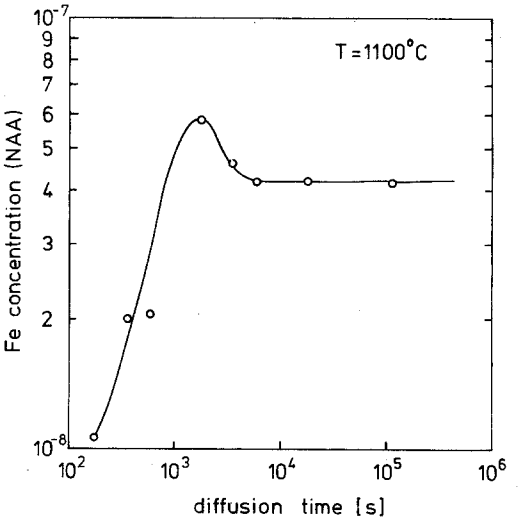

Fig. 3. Diffusion time dependence of the iron concentration in Fe plated silicon, $4 \times 4 \times 15$ mm^3, at 1100 °C [8]

diffusion time at 1100 °C [8]. The effective diffusion coefficient can be roughly estimated from the time necessary for 50 % saturation. The concentration maximum occuring after short diffusion times is due to insufficient boundary phase formation (Sect. 3.1).
The metal concentrations as measured by NAA and, for Cr, Mn, and Fe as well by EPR, do not increase even for long diffusion times (Fig. 3). The high diffusivities combined with fast establishment of the saturation concentration point to *predominantly interstitial diffusion* for these 3*d* metals in silicon.
The literature describes diffusion mechanisms other than interstitial diffusion for transition metals in Si as well, e.g. [50, 56, 62–64]. The dissociative mechanism proposed by Frank and Turnbull [65] for copper diffusion in germanium combines fast interstitial diffusion with a notable substitutional solubility. Substitutional diffusion is several orders of magnitude slower than interstitial (Fig. 2) so that the interstitial solubility limit will be reached fast. The time dependence of a substitutional concentration is thus determined by the availability of native lattice defects necessary for the transition from interstitial to substitutional sites. If the substitutional solubility happens to be higher than the interstitial, the diffusion time dependence of the total concentration is determined by the diffusion of native lattice defects whose equilibrium concentration is low [56, 59, 60].
This mechanism is considered for gold diffusion in Si where indeed saturation times are very long, e.g. 24 h at 1100 °C [66]. There is hope that exact measurement of the diffusion time dependence allows a decision in the controversy on the type of the dominant native lattice defect in Si [57]. However, it is not yet clear if at all isolated substitutional Au atoms are the electrically active species as generally assumed. Recent studies indicate a complex nature of the Au center in silicon [67] and EPR experiments only exhibited Au–Fe complexes in Au diffused silicon [59, 68, 69] even when using especially clean diffusion treatments [70]. Thus the microscopic nature of the dominant gold center in silicon may be further debated.
A dissociative diffusion mechanism is as well considered for Si:Ni [50, 62, 63]. The maximum concentration of Ni in silicon is reached even at 700 °C within 2 min (NAA result [10]). Electrical measurements, however, show a defect whose concentration slowly increases with diffusion time. This defect is ascribed to substitutional Ni [62, 63] (Sect. 4.1.7). It occurs in concentrations several orders of magnitude lower than the total Ni concentration, so that even in this case the dominant diffusion mechanism for the total Ni concentration is purely interstitial diffusion.
A high metal concentration close to the sample surface has been detected after long diffusion times in most diffusion experiments with transition metals in silicon. Occasionally this has been taken as evidence for a slowly diffusing species, probably substitutional 3*d* metals of high solubility, e.g. by Collins and Carlson for Si:Fe [64]. However, this common effect has rather to be ascribed to surface induced gettering and precipitation during quenching, [24, 71–73].
In conclusion, *these results prove interstitial diffusion – independent of native lattice defects – to be the dominant diffusion mechanism for the* 3*d elements* Cr, Mn, Fe, Co, Ni, *and* Cu *in silicon.* However, the existence of a small substitutional fraction of these elements cannot be ruled out by the present results. For those species the model of dissociative diffusion may apply.

2.3. *Diffusivity Near Room Temperature*

Quenching of T-metal diffused silicon changes the state of the interstitial atoms from thermal equilibrium into a highly supersaturated solution, the solubility at room temperature being in all cases considered less than one atom/cm^3 (extrapolation of the solubility results, Sect. 3.2). These interstitials are mobile even down to room temperature [1], so that a fraction (from Cr, Mn, and Fe) or virtually all of them (Co, Ni, and Cu) are lost during or immediatly after the quench. They form preferably silicide precipitates (e.g., Si:Cu [74, 75], Si:Ni [52, 76], Si:Co [24], Si:Fe [77]). These silicides can shorten *p/n* junctions and so severely disturb the electrical performance of silicon devices [77, 78].
Metal atoms remaining in interstitial sites after quenching (V_i, Cr_i, Mn_i, Fe_i) may be quite stable showing room temperature "decay times" of the order of months in *i*-Si [79]. For Fe this holds as well in *n*-Si [80]. The high stability despite the obvious room temperature mobility reflects the perfection of silicon crystals, offering no precipitate nucleation site whithin several μm diffusion length, as can be estimated from the diffusion coefficient (Fig. 4).
All 3*d* metals form donor levels so that they are positively charged in *p*-Si (Sect. 4.1). Their diffusivity is not noticeably charge state dependent. These mobile ions can be captured by negatively charged (substitutional) shallow acceptors, e.g. as $(Fe_i^+ B_s^-)$-pair. Those donor-acceptor pairs are well known from EPR experiments [1]. It has been proved that they indeed are formed only if Coulomb attraction is present: In phosphorus and boron co-doped but still *n*-type silicon no (FeB) pair formation is observed by EPR [79] as in this case Fe_i is in the neutral charge state Fe_i^0 and thus not attracted by B_s^-.
Pair formation at room temperature and up to 100 °C and dissociation at higher temperatures has been extensively studied for Si:Fe:B [6, 81–85]. It can be properly described within the framework developed by Reiss et al. [86] for (LiB) pairing, [83]. The pair

binding energy is close to 0.5 eV [83–85], in accordance with the simple point charge model [86]. Pair dissociation can be achieved by thermal treatment or by illumination with white light [6] at room temperature, but not at 100 K (EPR observation [82]) which can be taken as indication for a recombination enhanced process [87].

Deep level defects created and destroyed during (FeB) formation and dissociation in silicon result in instabilities of the electrical properties of these crystals [88]. EPR experiments combined with sheet resistivity measurements proved the correlation of (FeB) pair formation and dissociation processes with *resistivity changes amounting up to a factor of* 100 *during reversible thermal cycling* in the 20–150 °C range or by room temperature illumination with a 30 W incandescent bulb [79].

After quenching, only a fraction of Fe_i is paired with B_s, resulting in partial compensation (for $[Fe_i] < [B_s]$). The compensation and therefore the resistivity increase by further FeB pair formation during room temperature storage. These processes can be explained by the existence of a $(Fe_iB_s)^{0/+}$ donor level (Sect. 4.1.5), each isolated Fe_i atom compensating one shallow acceptor, each paired Fe atom in effect two, as long as the Fermi level is below the $(FeB)^{0/+}$ donor. The quantitative results of Shepherd and Turner [88] are correct despite wrong assumptions regarding the (FeB) levels, because additionally this double compensation effect was neglected. Dissociation of pairs by a heat treatment or illumination is connected with reappearance of isolated Fe_i [6, 81] thus diminishing the compensation, and this process can be cycled.

Heating to higher temperatures results in irreversible loss of Fe_i supposedly by precipitation. As interstitial iron is a common defect in heat treated silicon [7, 89] effects as described above might be frequently observed without being properly understood.

The diffusivity of interstitial iron near room temperature corresponds to a diffusion coefficient in the 10^{-15} cm^2/s range [40, 83, 88, 90]. This value is at least two orders of magnitude higher than an extrapolation of Struthers' data [39] (Table 1). However, Struthers determined only four diffusion coefficients (!) in the small temperature range of 1100–1250 °C. Moreover these values scatter so that an extrapolation down to room temperature, e.g. [40, 83], is questionable.

Figure 4 demonstrates that Struthers' values and the low temperature diffusion coefficients can be consistently explained by the expression:

$$D(\mathrm{Fe_i}) = 1.3 \times 10^{-3} \exp(-0.68\,[\mathrm{eV}]/kT)\,[\mathrm{cm^2/s}] \quad (3)$$

obtained from a least square fit of all diffusivity results for Fe in Si [39, 40, 83, 88, 90]. The activation energy of 0.68 eV thus derived is identical with an EPR value

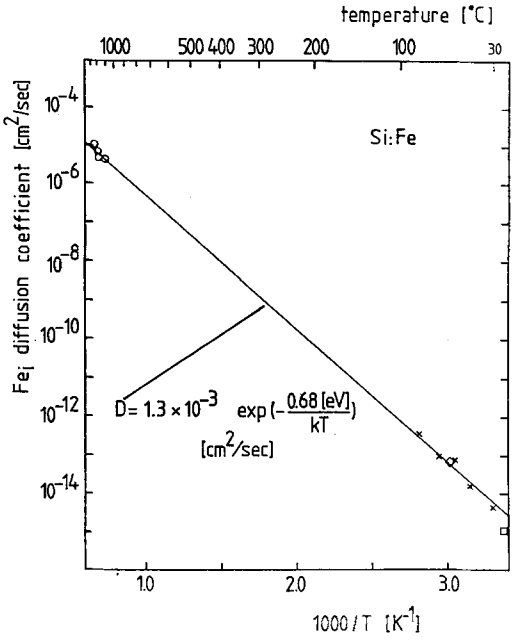

Fig. 4. Diffusion coefficient of interstitial iron in silicon, obtained by radiotracer diffusion experiments (○) [39] at high temperatures, and DLTS (◇) [83], resistivity (×) [88], and EPR (□) [90] measurements at low temperatures. The least square fit has been performed using all these results

obtained from low temperature annealing of Fe_i^0, Lee et al. [89]. Most of the other low temperature data correspond to Fe_i^+ diffusivities so that no charge state dependence of D can be stated.

The diffusion coefficient for interstitial diffusion of iron in silicon, (3), can be regarded as the most precise determination of all 3*d* metals in silicon as it is calculated out of data spanning 10 orders of magnitude in D. Any assumption of different diffusion mechanisms for iron in silicon at low and at high temperatures [83] thus appears to be obsolete. The same has been concluded for Cr_i in Si by Bendik et al. [37].

2.4. *Theory of Interstitial Diffusion*

The diamond lattice of silicon is an open structure so that interstitial diffusion should not depend primarily on lattice strains produced during movement of the diffusant from one interstitial site to the next. Swalin [91] therefore proposed the activation energy for interstitial diffusion to be determined mainly by Coulombic interaction with imperfectly screened host atoms. He calculated the sum of these interaction energies U_{ij} for an interstitial atom i and the nearest host atoms j (55 taken into account) at a distance d_{ij}

$$\sum U_{ij} = \sum z_i z_j e^2/\varepsilon d_{ij}, \quad (4)$$

using effective valences z_i, z_j obtained by means of semi-empirical screening considerations of Pauling

[92] (ε: dielectric constant). This calculation is carried out for the two different interstitial positions in the silicon lattice, having tetrahedral and hexagonal symmetry, respectively. The activation energy of interstitial diffusion should correspond to the energy difference between these sites. For instance, motion from one tetrahedral site to the next necessarily involves passing through the hexagonal configuration or vice versa, if the hexagonal site is the stable configuration.

Although Swalin's model is only a very simple picture, the resulting activation energies are in the range of 1 eV and less, using no adjustable parameters. More elaborate approaches like that of Weiser [93] which were discussed in Hu's review [34] do not give better agreement for the activation energies but determine the D_0 values reasonably. The entropy contribution to D_0 can be neglected corresponding to only small disorder around an interstitial T-metal.

For Fe_i in Si no charge state dependence of the diffusion coefficient could be found. This seems to contradict Swalin's assumption that electrical forces determine the activation energy of interstitial diffusion. However, self consistent Hartree-Fock calculations for transition metal ions in silicon by Haldane and Anderson [94] show only very small changes of the effective charge in the core region of the T-metals when the occupancy of *d*-states is changed considerably. This is explained by hybridization of *d*-states with silicon band states. A similar conclusion has been derived recently by Zunger et al. [95] using the quasi band Green's function method. From these results indeed no great influence of the charge state on the activation energy of diffusion can be expected.

3. Solubilities of 3*d* Transition Metals in Silicon

Results of solubility studies have rarely been used for theoretical analysis, in contrast to diffusion data. The available experimental solubility values of impurities in silicon obviously were not yet reliable enough. Since Trumbore's work [3] no new review papers on this subject have been published whereas numerous reviews exist on diffusion in semiconductors like Hu's paper [34]. In this paragraph solubility curves for the 3*d* elements Cr, Mn, Fe, Co, Ni, and Cu are presented in Figs. 5–11 and Table 2. For these elements new data have been established by systematic NAA and, whenever possible, EPR investigations [8–11]. All data used are based on experiments with small shallow doping (below $10^{16}\,cm^{-3}$).

Figure 5 shows for the solubilities the same general trend within the 3*d* row as Fig. 2 for the diffusivities: increasing values with increasing atomic number. In the following, first the thermochemical boundary conditions corresponding to these solubility data are

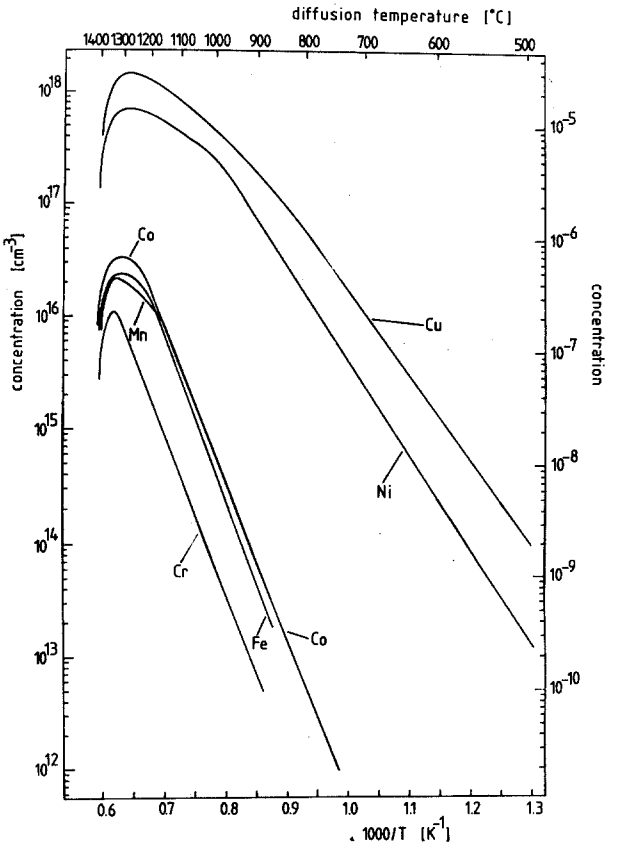

Fig. 5. Solubilities of 3*d* metals in silicon, collected from Figs. 6–11. The curves are calculated as described in Sects. 3.2 and 3.3

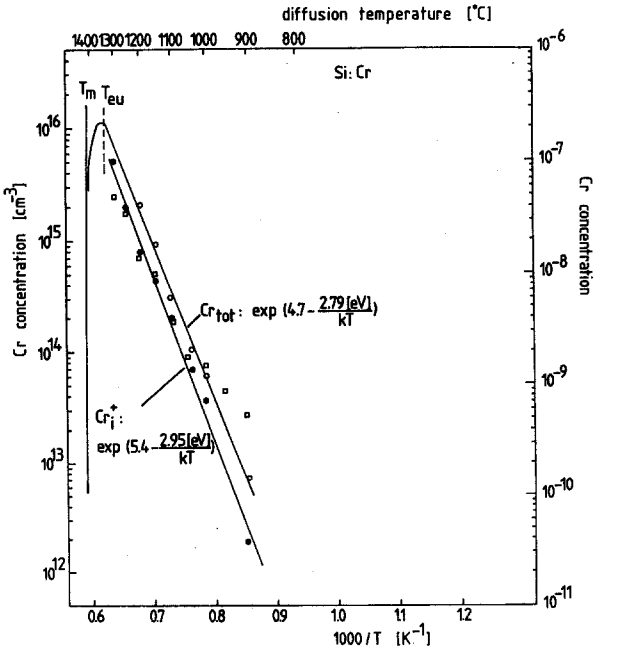

Fig. 6. Solubility of Cr in silicon as measured by NAA (Cr_{tot}) (○) and EPR (Cr_i^+) (●) of suitably doped *p*-Si [9–11, 129]. Further included are NAA data (□) of Würker et al. [101]

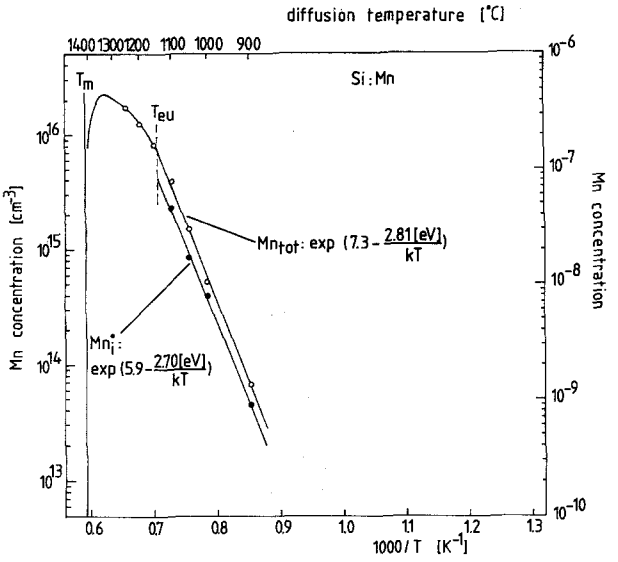

Fig. 7. Solubility of Mn in silicon, measured by NAA (Mn_{tot}) (○) and EPR (Mn_i^0) (●) [10, 11]

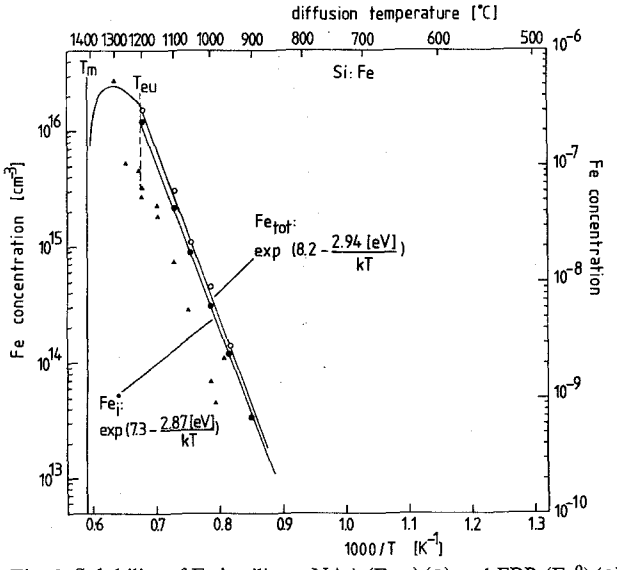

Fig. 8. Solubility of Fe in silicon, NAA (Fe_{tot}) (○) and EPR (Fe_i^0) (●) data [8] compared with Struthers' [39] radiotracer results (△). EPR results of Lee et al. [89] are well in accordance with these data

considered. In Sects. 3.2 and 3.3 appropriate thermochemistry is used for evaluation of the experimental results. A discussion of all findings is given in Sect. 3.4.

3.1. Boundary Conditions

Solubilities of solutes in a solvent, solid silicon in this case, are defined in equilibrium with a boundary phase. Using metal plated samples such as described in Sect. 1.1, at diffusion temperatures above the eutectic temperature of the respective silicon-metal phase diagram ([103, 104], see Table 2) the equilibrium boundary phase is the melt formed at the silicon-metal

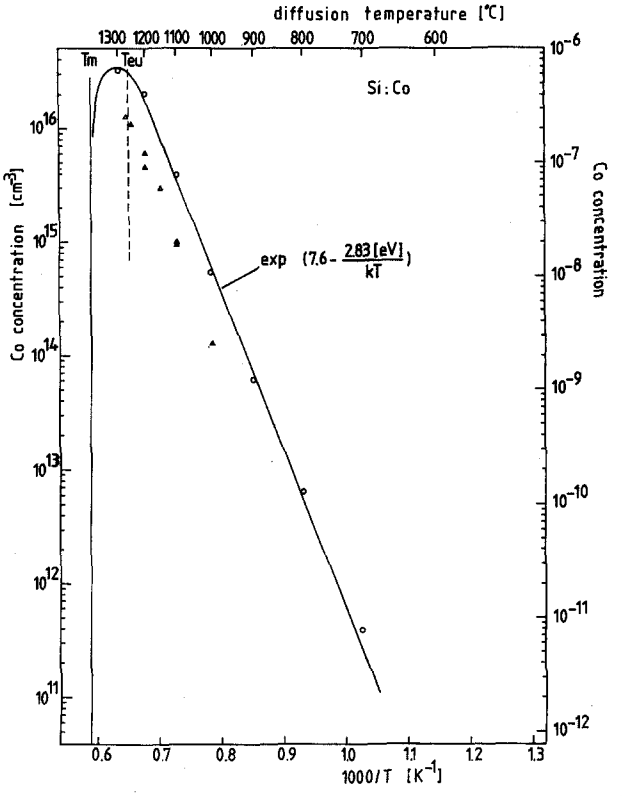

Fig. 9. Solubility of Co in silicon, NAA results [9–11] (○) and radiotracer data of Kitagawa et al. [49] (△)

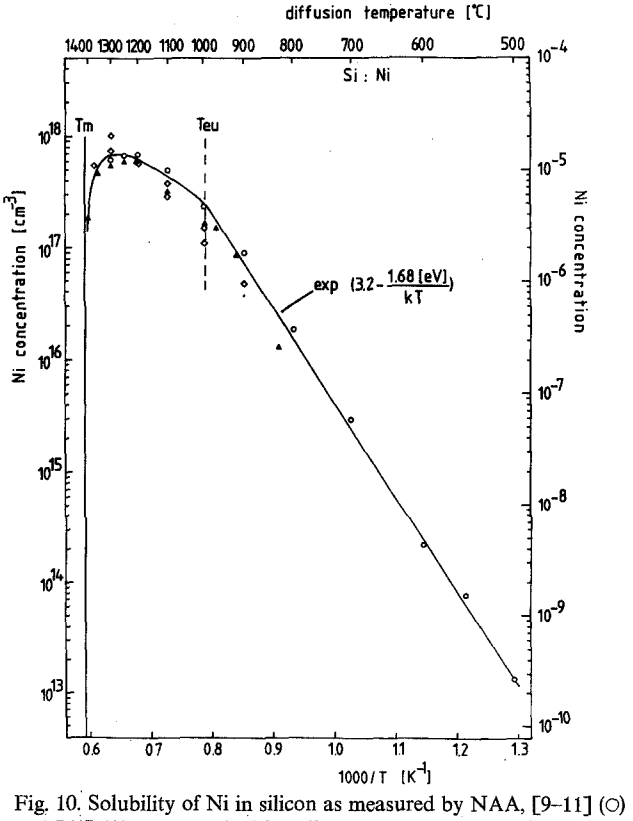

Fig. 10. Solubility of Ni in silicon as measured by NAA, [9–11] (○) and [51] (◇), compared with radiotracer measurements (△) [52]

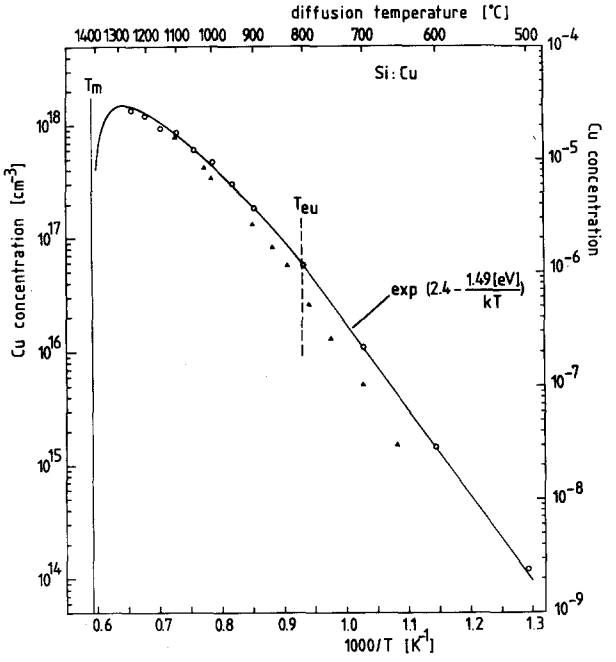

Fig. 11. Solubility of Cu in silicon, determined by NAA: (○) [11] and (△) [99]. NAA results at $T < T_{eu}$ of [99] are obtained by equilibration with Cu_3Si whereas those of [11] correspond to a metal layer as boundary phase (Sect. 3.1). Further radiotracer data [43, 100] are included in Table 2

interface. Below the eutectic temperature thermal equilibrium depends on the formation of a solid silicon-rich silicide at the interface layer.

This problem has been addressed by Dorward and Kirkaldy [99] for the Si:Cu system. They compared solubilities obtained by the usual "plate and anneal" technique described in Sect. 1.1 with those measured by heat treatment of silicon samples together with powdered Cu_3Si in a closed capsule. In the first case a concentration maximum like that shown in Fig. 3 for Si:Fe was observed (after, e.g., 9 h at 700 °C for Si:Cu). Subsequently the total concentrations decreased and reached finally the equilibrium value determined by the second technique. Whereas at the maximum equilibrium can be assumed to correspond to the metal layer covering the sample, for long diffusion times equilibrium with the silicide formed at the silicon-metal interface is established. The maximum occurs from a greater saturation concentration with pure metal as boundary phase compared to silicide, because in the latter case the effective enthalpy of formation is higher due to the silicide formation (Sect. 3.4.2).

Formation of interface silicides is extensively investigated as it is important for Schottky contact formation, see e.g. a recent review by Tu and Mayer [105]. As an example, 20 min heating at 300 °C of a Ni plated sample results in Ni_2Si formation, at 350 °C in NiSi, and at 840 °C finally in $NiSi_2$ (Rutherford backscattering result [106]). The high temperature silicon-rich silicide is for all 3*d* elements from Ti to Ni of the type MSi_2 [103–105], but for Si:Cu, Cu_3Si [107].

From the diffusion temperatures and times used for the EPR/NAA study [8–11] for Cu and Ni at $T < T_{eu}$(500–800 °C) it must be expected that those data represent solubilities with metal as boundary phase. For Co, Fe, Mn, and Cr with higher diffusion temperatures at $T < T_{eu}$(800–1200 °C), equilibrium with the respective silicide can be reached, the data of Figs. 6–9 representing final equilibrium values as demonstrated in Fig. 3 for Si:Fe. First, the solubilities for $T < T_{eu}$ will be considered.

3.2. Solubilities Below the Eutectic Temperatures

From the equilibrium condition of equal chemical potential of each component (1, 2) in each phase of a two phase (α, β) solid state system can be deduced

$$\ln(x_2^\alpha / x_2^\beta) = \Delta S_2^{\alpha,\beta}/k - \Delta H_2^{\alpha,\beta}/kT \tag{5}$$

with x_2^α being the concentration of component 2 in phase α, $\Delta S_2^{\alpha,\beta}$ the relative partial excess entropy, $\Delta H_2^{\alpha,\beta}$ the relative partial excess enthalpy of the solute 2 in phase α, with respect to phase β and k the Boltzmann constant. This means, $\Delta H_2^{\alpha,\beta}$ is the energy required to transfer an atom of species 2 from phase β into phase α, $\Delta S_2^{\alpha,\beta}$ is the entropy change associated with this process. Denoting phase α with solid silicon (superscript s) and β with the solid silicide or metal (superscript i), respectively, the concentration x_2^i is independent of temperature and (5) gives an Arrhenius type temperature dependence for the saturation concentration x_2^s. This indeed is observed for $T < T_{eu}$ (Figs. 6–11 and Table 2):

$$\ln x_2^s = \Delta S_2^{s,i}/k - \Delta H_2^{s,i}/kT. \tag{6}$$

Cr, Mn, and Fe (Figs. 6–8), for which quantitative EPR measurements were possible, yield *the same enthalpy of formation* $\Delta H_2^{s,i}$ (~2.85 eV) *within experimental uncertainty for interstitial ions present in the samples after quenching* (EPR) *as well as for the total concentration* (NAA). This equal enthalpy of formation indicates that both techniques measure properties of the same species: interstitial transition metal atoms in silicon. The absolute difference between both concentrations is mainly due to loss of a part of these interstitials during the quench.

Table 2. Solubility data of 3*d* elements in silicon. (Atomic concentrations x_2 are converted via: $c_2 = 5 \times 10^{22}\, x_2$ [cm^{-3}])

Metal	$T < T_{eu}$: metal concentration $\ln x_2^s = \Delta S_2^{s,i}/k$	$-\Delta H_2^{s,i}/kT$ [eV]	Special concentration c_2 (1100 °C) [cm^{-3}]	x_2^s(max)	$T > T_{eu}$: distribution coefficient $\ln k = \ln x_2^s/x_2^l = \Delta S_2^{s,l}/k$	$-\Delta H_2^{s,l}/kT$ [eV]	$k_m = k$ (1685 K)	Method	Ref.	Eutectic temperature T_{eu} [K] [103, 104]
Ti	3.9	3.0	2×10^{13}					DLTS	[96][b]	1603
V			$\sim 10^{13}$					DLTS	[97][b]	
Cr	4.7	2.79	3×10^{14}	2×10^{-7}	1.0[c]	2.0[c]	3×10^{-6}[c]	NAA	[9–11][e]	1608
	Cr_i^+: 5.4	2.95						EPR	[9–11]	
Mn	7.3	2.81	3×10^{15}	4×10^{-7}	1.2	1.92	6×10^{-6}	NAA	[10, 11][f]	1415
	Mn_i^0: 5.9	2.70						EPR	[10, 11]	
Fe	8.2	2.94	3×10^{15}	5×10^{-7}	1.0[c]	1.86[c]	7×10^{-6}[c]	NAA	[8]	
	Fe_i^0: 7.3	2.87						EPR	[8]	1479
	7.9[a]	3.1[a]						Tracer	[39]	
Co	7.6	2.83	4×10^{15}	7×10^{-7}	1.0[c]	1.76[c]	1.5×10^{-5}[c]	NAA	[9–11][f]	1532
	7.5[a]	2.99[a]						Tracer	[98]	
Ni	3.4	1.68	5×10^{17}	1×10^{-5}	−1.4	1.08		NAA	[9–11]	
					−0.71	1.20		Tracer	[72]	1266
					1.9[a]	1.51[a]		NAA	[51]	
					−0.17[d]	1.25[d]	1.5×10^{-4}	Various[d]		
Cu	2.4	1.49	9×10^{17}	3×10^{-5}	−0.35	1.17		NAA	[11]	
					2.1	1.46		NAA	[99]	
	0.1	1.39						Tracer	[43]	1075
					1.6	1.41		Tracer	[100]	
					1.0[d]	1.35[d]	2.5×10^{-4}	Various[d]		

[a] Derived out of data and figures of the respective reference
[b] For Si:Ti and Si:V only electrical data are available at present
[c] Extrapolated values from $T < T_{eu}$, assuming $\Delta S_2^{s,l} = 1\ k$ (Sect. 3.3)
[d] Best fitting of all results (Fig. 14 for Si:Ni)
[e] Cr solubilities of Würker et al. [101] do not follow an Arrhenius law (Fig. 6); Cr_i^+ concentrations determined by Feichtinger et al. [102] (EPR) cannot be considered as solubility values, as discussed in that reference
[f] Solubility data of Bakhadyrkhanov et al. for Si:Mn [38] and Si:Co [41] are comparable in magnitude with other references; yet the differences, especially regarding the slope of Arrhenius plots (enthalpies of formation), are considerably so that these tracer data are not included

Combined with the already discussed observations on the time dependence of the in-diffusion process (Sect. 2.2), the important conclusion is reached that *all these 3d metals not only diffuse interstitially into silicon but as well stay preferably in interstitial sites in thermal equilibrium at high temperatures.* The quantitative results of formation enthalpies and entropies will be discussed in Sect. 3.4.

3.3. Solubilities Above the Eutectic Temperatures

For further evaluation of solubilities obtained at temperatures above the respective eutectic temperature, some further thermochemistry is necessary, as the reference state now is the strongly temperature dependent liquid phase. The concentration symbols used are illustrated in a schematic phase diagram (Fig. 12).

Neglecting the small difference in heat capacity between solid and liquid [108] and treating the solution of the metal in the liquid silicon as ideal solution [109], (5) has now to be written as

$$\ln(x_2^s/x_2^l) = \ln k = \Delta S_2^{s,l}/k - \Delta H_2^{s,l}/kT, \qquad (7)$$

with $\Delta S_2^{s,i}$, $\Delta H_2^{s,i}$ being the excess partial entropy and enthalpy of the solute in the solid phase with respect to

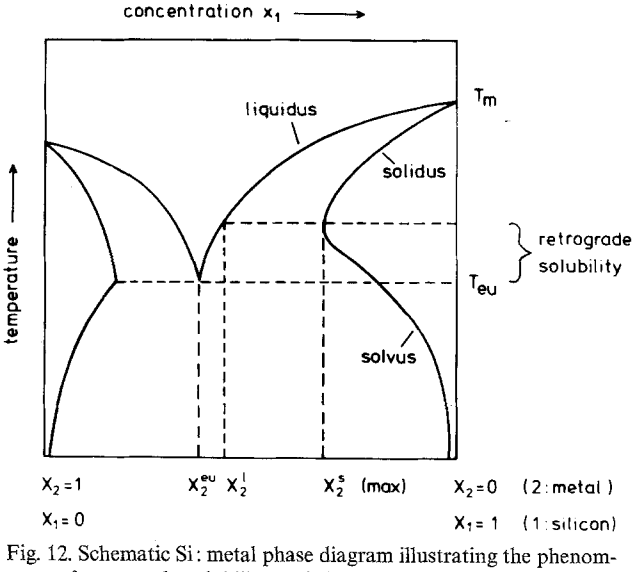

Fig. 12. Schematic Si: metal phase diagram illustrating the phenomenon of retrograde solubility and the usual solubility maximum at the eutectic temperature

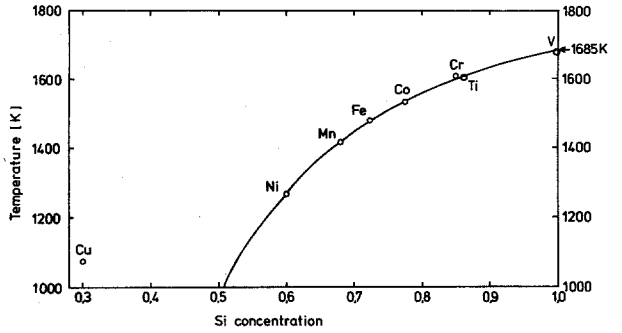

Fig. 13. Eutectic temperatures and compositions of Si:3*d* metal systems [103, 104]. For all metals forming silicon-rich silicides of the type MSi_2 (Ti–Ni) these values turn out to be on one liquidus line described by the parameters of (13). Si:Cu forming only Cu_3Si [107] is markedly different

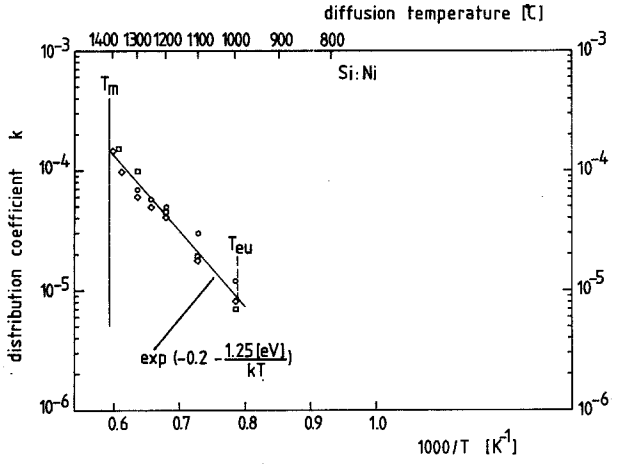

Fig. 14. Temperature dependence of the Si:Ni distribution coefficient, calculated by means of the liquidus curve given in Fig. 13. The solubility values used (Fig. 10) are NAA results, (○) [9–11] and (□) [51] and radiotracer data [52] (◇). The least square fit has been obtained from all these values

the liquid phase (superscript l). The distribution coefficient at the silicon melting point, $k_m = k(T = T_m)$ is the technologically important "segregation coefficient". Experimentally determined are solid solubilities $x_2^s(T)$. The distribution coefficient can only be obtained via evaluation of the "liquidus" $x_2^l(T) = 1 - x_1^l(T)$. For an ideal, silicon rich solution the liquidus curve is simply given by, [108],

$$\ln x_{1\,\mathrm{id}}^l = \Delta S_1^m/k - \Delta H_1^m/kT. \tag{8}$$

The data used for silicon are [110]:

melting point: $T_m = 1685\,\mathrm{K}$,

enthalpy of fusion: $\Delta H_1^m = 0.525\,\mathrm{eV}$,

entropy of fusion: $\Delta S_1^m/k = \Delta H_1^m/kT = 3.62$.

However, the liquidus curves of Si:T-metal phase diagrams [103, 104] are clearly non-ideal, [111]. This can be taken into account by an activity coefficient γ_1^l:

$$\ln x_1^l \gamma_1^l = \ln x_{1\,\mathrm{id}}^l = \Delta S_1^m/k - \Delta H_1^m/kT \tag{9}$$

so that

$$\gamma_1^l = x_{1\,\mathrm{id}}^l/x_1^l. \tag{10}$$

In general, the activity coefficient γ_1^l, being unity at the melting point of the solvent 1, temperature and composition dependent. It can be expressed using a relative partial excess entropy $\Delta\tilde{S}$ and enthalpy $\Delta\tilde{H}$ [111]:

$$\ln \gamma_1^l = \Delta\tilde{S}/k - \Delta\tilde{H}/kT. \tag{11}$$

Thurmond and Kowalchik [111] analysed various liquidus curves of germanium and silicon phase diagrams and found in most cases $\Delta\tilde{S}$ and $\Delta\tilde{H}$ to be proportional to $(1-x_1^l)^2 = (x_2^l)^2$. For Si:Cu they determined

$$\begin{aligned} &\Delta\tilde{H} = 0.52\,(x_2^l)^2\ [\mathrm{eV}], \\ &\Delta\tilde{S} = 3.62 (x_2^l)^2 k \quad \text{(boundary silicide: } Cu_3Si). \end{aligned} \tag{12}$$

Own analysis of the liquidus lines in the Si:T-metal phase diagrams [103, 104] resulted in various parameters (12) for the 3*d* elements. These determinations are very sensitive to not exactly drawn liquidus lines (e.g. that of Si:Mn [104] terminates at a silicon melting point of 1733 K!). However, for all 3*d* elements from Ti to Ni the more carefully determined eutectic temperatures and compositions lie on one single liquidus curve (Fig. 13). In a least square fit the following parameters could be deduced

$$\begin{aligned} &\Delta\tilde{H} = 1.41\,(x_2^l)^2\ [\mathrm{eV}], \\ &\Delta\tilde{S} = 8.68\,(x_2^l)^2 k \quad \text{(boundary silicide: } MSi_2). \end{aligned} \tag{13}$$

With these parameters the liquidus line in Fig. 13 was calculated, using (9) and (11). The unexpected result, that the liquidus lines for all 3*d* elements forming MSi_2 silicides (Ti to Ni) can be described by identical parameters, allows to conclude on comparable interaction parameters in the liquid state for these elements.

By means of the values x_2^l for the liquidus curves, now the solid solubilities x_2^s of Si:Mn, Si:Ni, and Si:Cu (with the lowest eutectic temperatures) can be converted into distribution coefficients, (7), using the liquidus parameters (13) and (12), respectively (Table 2). As an example, the result is demonstrated for Si:Ni (Fig. 14). The distribution coefficient indeed follows an Arrhenius type law, (7), up to the melting point. The maximum of the solid solubility (Fig. 10) is determined mainly by the liquidus curve x_2^l which necessarily approaches 0 at the melting point of pure silicon. The phenomenon of retrograde solubility, i.e. the occurrence of this maximum solubility at a temperature higher than the eutectic temperature, will be

analyzed in Sect. 3.4.1. Similarly the data for Si:Cu and Si:Mn could be fitted, the results are included in Table 2.

For the other 3*d* metals an estimation of the distribution coefficient above the respective eutectic temperature was possible by assuming for these elements an effective excess partial entropy of $\Delta S_2^{s,1} \sim 1k$ with respect to the liquid state. This assumption is based on the results for Mn ($1.2k$), Ni ($-1.4k$ to $1.9k$), and Cu ($-0.35k$ to $2.1k$), see Table 2. The effective partial enthalpy $\Delta H_2^{s,1}$ now can be determined using the value $\kappa(T_{eu})$ known from the low temperature data of Table 2.

Now complete solidus curves up to the melting point can be calculated, using (7), (9), and (11) with the parameters of Table 2 and (12) or (13), respectively. These curves are drawn in Figs. 5–11. The experimentally determined solubilities are satisfactorily described in this way. All solubility curves show a maximum. For Si:Cr the temperature of this maximum coincides with the eutectic temperature. This system behaves "normal" (Fig. 12, left-hand side) and does not show retrograde solubility in the common meaning, [112]. This will be treated shortly in the next subsection.

3.4. Discussion of Solubilty Results

3.4.1. The Solid Solubility Maximum. The maximum solid solubilities of impurities in silicon are related with the melting point distribution coefficients κ_m according to an empirical relation found by Fischler [113]:

$$x_2^s(\max) \cong 0.1\,\kappa_m. \tag{14}$$

Table 2 demonstrates that this holds quite well for the 3*d* elements in a two-orders-of-magnitude concentration range. Instead of the theoretical explanation given by Statz [114] based on a theory of Lehovec [115] a more transparent treatment without introduction of new parameters is possible:

The distribution coefficient at the melting point is given by (7):

$$\kappa_m = \exp(\Delta S_2^{s,1}/k - \Delta H_2^{s,1}/kT_m). \tag{15}$$

In order to calculate the temperature of maximum solid solubility, which is close to the melting point (Fig. 5), the liquidus x_1^l can be treated as ideal, using (8). Then by differentiation of

$$x_2^s = \kappa \cdot x_2^l = \kappa \cdot (1 - x_1^l) \tag{16}$$

with $\kappa(T)$ given by (7), the temperature of maximum concentration comes out to

$$T(x_2^s(\max)) = \frac{\Delta H_1^m/k}{\Delta S_1^m/k - \ln\left(\dfrac{\Delta H_2^{s,1}}{\Delta H_2^{s,1} + \Delta H_1^m}\right)}. \tag{17}$$

The corresponding maximum solubility $x_2^s(\max)$ can be calculated using (16), (7), (9), (11), and (12) or (13), respectively. Numerical evaluation of these maximum solubilities and of the corresponding segregation coefficients, (15) shows that Fischler's relation (14) indeed is valid for a wide range of formation enthalpies: it is exactly fulfilled for $\Delta H_2^{s,1} = 1.7$ eV, and $\Delta H_2^{s,1}$ between 1 eV and 3.5 eV result in $x_2^s(\max)/\kappa_m$ between 0.15 and 0.05. As all 3*d* elements yield $\Delta H_2^{s,1}$ in the range 1.2–2 eV (Table 2) they are indeed expected to follow (14). This treatment demonstrates Fischler's relation to be a consequence of quite simple thermochemistry.

Now, the question of retrograde solubility (Fig. 12) can be elucidated in a quantitative way: *Retrograde solubility is observed, if the enthalpy of formation $\Delta H_2^{s,1}$ is so large that the temperature determined by* (17) *is higher than the eutectic temperature.* For Si:Cr, taking $\Delta H_2^{s,1} = 2.0$ eV (Table 2) (17) *yields* a temperature for the maximum solubility of 1580 K, which indeed is lower than the eutectic temperature (1605 K [104]). For this system no retrograde solubility can be expected, the actual solubility maximum coinciding with the eutectic temperature. The same holds for Si:Ti and Si:V because of their high eutectic temperatures (Table 2). For the other 3*d* elements (Mn–Cu) retrograde behaviour is predicted in agreement with the observations.

3.4.2. Distinction of 3d Elements Into Two Groups. The excess partial entropies and enthalpies derived from distribution coefficients, (7), describe the equilibrium between metal atoms in solid silicon and in the liquid state. Thus they contain the enthalpy ΔH_2^m and entropy ΔS_2^m of fusion of the respective metal [99, 100] (the solution of the metal in the melt treated as ideal [109]):

$$\Delta H_2^{s,1} = \Delta H_2^s - \Delta H_2^m, \tag{18}$$

$$\Delta S_2^{s,1} = \Delta S_2^s - \Delta S_2^m. \tag{19}$$

For the 3*d* elements holds, [116],

$$\Delta H_2^m = 0.18 \pm 0.04\,\text{eV}, \qquad \Delta S_2^m = 1.1 \pm 0.1k. \tag{20}$$

This way the *partial enthalpies ΔH_2^s and entropies ΔS_2^s of an interstitial solution of a 3d metal atom in solid silicon*, which may be called formation enthalpies and entropies, come out to:

for Cu, Ni:

$$\Delta H_2^s = 1.5 \pm 0.1\,\text{eV}, \qquad \Delta S_2^s = 2.0 \pm 0.5k \tag{21}$$

for Mn and most probably as well for Co, Fe, and Cr:

$$\Delta H_2^s = 2.1 \pm 0.1\,\text{eV}, \qquad \Delta S_2^s = 2.0 \pm 0.5k. \tag{22}$$

For the elements represented by Mn, the difference between the low temperature data (equilibrium with the silicide):

$$\Delta H_2^{s,i} = 2.85 \pm 0.1\,\text{eV}, \quad \Delta S_2^{s,i} = 7 \pm 1k \tag{23}$$

and the values of (22) must be related to the enthalpy and entropy of formation of the respective silicide. These amount to $\Delta H_2^f = 0.8$–$1.1\,\text{eV}$ and $\Delta S_2^f = 6$–$8k$ [105, 116] per molecule. For each metal atom entering the silicon crystal one MSi_2 molecule has to be dissociated. As expected, the difference between (22) and (23) agrees within the error limits with these silicide formation parameters. For Cu and Ni, however, equilibrium with the pure metal can be assumed (Sect. 3.1) so that the respective low temperature values, Table 2, are close to those obtained at high temperatures, (21).

These enthalpies of formation allow to *distinguish the 3d metals into two subgroups*:

3dI: Cr, Mn, Fe, and Co showing $\Delta H_2^s = 2.1 \pm 0.1\,\text{eV}$

and

3dII: Ni and Cu with $\Delta H_2^s = 1.5 \pm 0.1\,\text{eV}$.

Concerning the other 3*d* elements only little information is available. DLTS measurements [96, 97] indicate Ti and V to belong to the 3*dI* group. The solubility of 3*dII* elements is markedly higher than that of 3*dI* elements (Fig. 5), because of smaller formation enthalpy, combined with similar formation entropy, (21) and (22).

It is interesting to note that a distinction between Fe, Cr, and Co on the one side and Cu and Ni on the other has been observed for the formation of "haze" defects (etching figures from metal precipitates) on heat treated silicon wafer surfaces as well [117], the 3*dII* elements showing more pronounced haze formation. Similarly, Buck et al. [118] report of a distinction of Fe, Co, and Au against Cu and Ni, in this case 3*dII* elements yielding more rapid gettering than the others, as measured by Rutherford backscattering. Whereas Buck et al. gave an explanation by high substitutional solubilities for Fe, Co, and Au, this effect might be related with the high diffusivity and the higher total solubility of 3*dII* elements compared with 3*dI* elements.

3.4.3. Theoretical Models. The distinction of 3*d* transition metals into two groups is not due to properties of the respective reference state, as the thermochemical data of the silicides from Ti to Ni are very similar (Fig. 13). For the obvious difference between 3*dI* (Cr, Mn, Fe, Co) and 3*dII* (Ni, Cu) elements in silicon two explanations shall be considered:

Firstly, according to the EPR data of Ludwig and Woodbury [1] (Fig. 1) interstitial 3*d* metals promote both 4*s* electrons into the 3*d* shell so that Co_i^0 has a $3d^9$ configuration whereas Ni_i^0 reaches the closed $3d^{10}$ shell. If Ni_i diffuses as neutral atom it can be expected that its closed shell $3d^{10}$ configuration has a smaller interaction with the host than the preceeding 3*d* metals. This may lead to the high diffusivity and solubility of Ni and Cu (especially as the latter seems to diffuse as Cu_i^+, see below).

An alternate explanation is possible using the approach of the *dielectric two-band model of covalently bonded solids*, developed by Phillips and Van Vechten (see [119] and references therein). It assumes the enthalpy of formation of an interstitial atom to be mainly determined by the energy necessary to accommodate the valence electrons of the interstitial atom in the semiconductor band states. A truly interstitial atom (no interstitially sharing place with a lattice atom) does not increase the number of lattice sites. The valence band states are therefore occupied. Thus the accommodation must involve an admixture of the wave functions of the Z outermost valence electrons with conduction band states being higher in energy than the respective free atom states (Z is the effective valence of the metal atom). At the diffusion temperature the Fermi level is in the middle of the energy gap, using small shallow doping ($< 10^{16}\,\text{cm}^{-3}$). Then the additional energy required for the outermost valence electrons of a neutral interstitial metal atom M amounts:

$$\Delta H^s(M_i^0) = Z \cdot \bar{E}_g/2. \tag{24}$$

$\bar{E}_g$ is the effective energy gap averaged over the k space [119]

$$\bar{E}_g(\text{Si}) = 4.8\,\text{eV} \tag{25}$$

so that

$$\Delta H^s(M_i^0) = 2.4\,\text{eV}. \tag{26}$$

Here and in the following, the effective valence Z of all these interstitial 3*d* elements will be taken as $Z = 1$ so that the energy required for the outermost of the 3*d* electrons determines the enthalpy of formation. Regarding the similarities in the thermodynamics of solution of 3*d* elements in silicon any other determination of Z appears to be inappropriate.

If the energy level of this outermost electron is shallow enough the atom will be ionized at the diffusion temperature. In this case the energy difference from the Fermi level E_f to the conduction band E_c will be gained

$$\Delta H^s(M_i^+) = \Delta H^s(M_i^0) - (E_c - E_f)/2 = 1.7\,\text{eV}. \tag{27}$$

Table 3. Electron energy levels of interstitial 3*d* metals and metal-boron pairs in silicon. For each level, the electronic configurations are given, according to the model of Ludwig and Woodbury [1] (Fig. 1). For Ti in silicon a microscopic identification is lacking (Sect. 4.1.1)

Metal	Acceptor level $M_i^{-/0}$	Donor level $M_i^{0/+}$	Double donor level $M_i^{+/++}$	Pair donor level $(M_iB_s)^{0/+}$	Ref.
Ti	$E_c-0.08$ eV ($3d^5/3d^4$)	$E_c-0.28$ eV ($3d^4/3d^3$)	$E_v+0.25$ eV ($3d^3/3d^2$)		[96, 97, 127]
V	$E_c-0.16$ eV ($3d^6/3d^5$)	$E_c-0.45$ eV ($3d^5/3d^4$)	$E_v+0.30$ eV ($3d^4/3d^3$)		[36, 97, 128]
Cr		$E_c-0.22$ eV ($3d^6/3d^5$)		$E_v+0.28$ eV	[2, 97, 102, 129]
Mn	$E_c-0.11$ eV ($3d^8/3d^7$)	$E_c-0.42$ eV ($3d^7/3d^6$)	$E_v+0.25$ eV ($3d^6/3d^5$)	$E_c-0.55$ eV (?)	[97, 128]
Fe		$E_v+0.385$ eV ($3d^8/3d^7$)		$E_v+0.10$ eV	[6, 84, 85, 97, 130, 131]

The results of this crude estimation [119] should be compared with the data of (21) and (22). The model as well as those values give partial enthalpies of formation of the solid solutions. The agreement of these data is surprisingly good, even more the difference between 3*dI* ($\Delta H_2^s \cong 2.1$ eV) and 3*dII* ($\Delta H_2^s \cong 1.5$ eV) formation enthalpies in silicon. Thus this model predicts diffusion of neutral interstitials for the 3*dI* elements Cr to Co and, supposedly, Ti and V, and of singly positively charged interstitials for the 3*dII* elements Ni and Cu.

An experimental proof of this hypothesis can be made at best by drift experiments, i.e. investigations of 3*d* metal diffusion in silicon with applied electric field. Energy levels, determined at low temperatures, do not necessarily allow to deduce reliably high temperature charge states as the energy levels can be strongly temperature dependent with respect to the allowed bands [119]. Generally, a shallow donor level like that of Li in silicon [5] will result in a positively charged state, a deep donor may lead to a neutral charge state to be predominant at the diffusion temperature. The available results of drift experiments [120, 121] confirm diffusion of a positively charged ion for Cu (and Li) in Si, and neutral interstitials for Fe (and Au) in agreement with the model discussed above. At present, this model seems to be more appropriate for an explanation of the 3*dI*/3*dII* distinction than the simple closed shell argument mentioned before.

Another theoretical approach for the calculation of interstitial solubilities has been put forward by Weiser [122]. He calculated the balance between attractive van-der-Waals type interactions and a repulsive potential for the different interstitial sites (tetrahedral and hexagonal) to deduce solubilities. However, as pointed out by Hu [34] and Van Vechten [119] this approach contains a number of unknown parameters so that its use appears to be misleading.

4. Energy Levels of 3*d* Transition Metals in Silicon

Transition metals in silicon are known since more than 25 years to form energy levels in the forbidden gap, [64]. These levels are called "deep" levels, because they are not close to one of the allowed bands. Valence electron wave functions of deep level impurities are localized and not composed out of split-off band states like in the case of "shallow" donors and acceptors. The distinction between shallow levels related to the adjacent bands and deep levels gets evident by hydrostatic pressure experiments (Sect. 4.1.9.). Deep levels may act as traps for carriers or as recombination centers and thus determine electrical properties of silicon devices.

Electrical effects of transition metal contaminations of silicon are a problem of great concern, especially for the use of cheap "solar grade" silicon for solar cells. Whereas impurity concentrations of 10^{16} cm^{-3} Cu or Ni do not severely degrade cell performance, 10^{15} cm^{-3} Cr, Mn, Fe or Co or even only 10^{14} cm^{-3} Ti or V may result in a 50% drop in cell efficiency [123–125].

Electrical data for transition metals in silicon are described in several hundred publications, most of which were reviewed by Milnes [126] and Chen and Milnes [5]. Conclusive identifications and established energy levels are, however, not available in general. The following section presents a critical survey of the presently accessible information. Table 3 and Fig. 15 summarize the energy levels which appear reliably confirmed, taking into account the conclusions on diffusivities, preferred lattice site etc. obtained in the preceeding chapters.

4.1. Experimental Results

4.1.1. Si:Ti. DLTS investigations of Ti-doped silicon [96, 97, 127] found two donor levels near $E_v+0.25$ eV

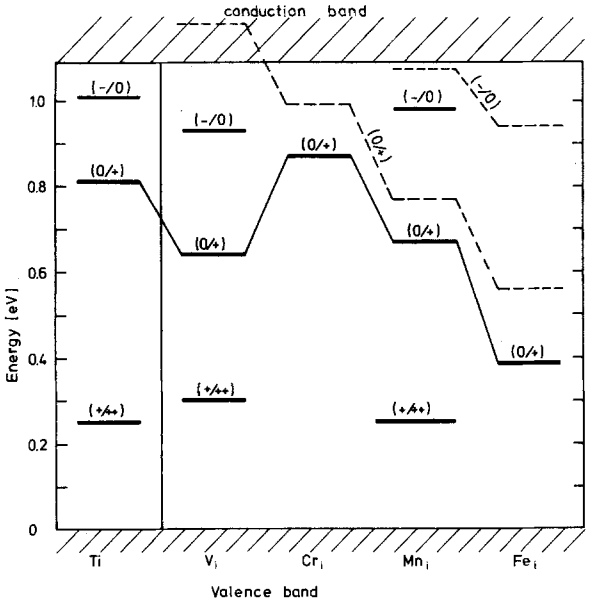

Fig. 15. Energy levels of interstitial 3*d* metals in silicon (full lines), see Table 3, compared with the results of X_α calculations of DeLeo et al. [15] (broken lines)

and $E_c-0.28$ eV, Graff et al. [97] additionally report a quite shallow acceptor at $E_c-0.08$ eV. The atomistic structure of this defect is not yet established by EPR. The "solubility curve" by Chen et al. [96] shows a similar slope (~ 3 eV) for electrically active Ti as that given in (23) for interstitial V, Cr, Mn, and Fe (Table 2), suggesting interstitial solution for Ti as well. However, present knowledge of the diffusion coefficient shows surprisingly low values for an interstitial diffusion mechanism. Therefore it cannot be excluded that Ti, which has four valence electrons, appears as substitutional species. Obviously, for this important lifetime killer in silicon solar cells [123–125] further investigations are badly needed.

4.1.2. Si:V. Vanadium in silicon has been detected by EPR as V_i^{++} [1] (Fig. 1). In addition to two donor levels an acceptor has been measured by Graff and Pieper [97] (DLTS) as well as by Ohta and Sakata [36] (DLTS and Hall effect) and Lemke [128] (DLTS and TSCA). All data agree quite well with

$$V_i^{-/0} \quad \text{at} \quad E_c-0.16\,\text{eV}, \tag{26}$$

$$V_i^{0/+} \quad \text{at} \quad E_c-0.45\,\text{eV}, \tag{27}$$

$$V_i^{+/++} \quad \text{at} \quad E_v+0.30\,\text{eV}. \tag{28}$$

V_i does not show room temperature instability [128] like Cr_i, Mn_i, and Fe_i. The diffusion coefficient seems to be considerably lower than that of the other 3*d* elements in silicon (expect Ti), probably causing the deleterious effect of V on solar cells (Sect. 4.1.9).

4.1.3. Si:Cr. EPR observations of Cr_i^0 and Cr_i^+ in silicon prove the existence of a donor level determined already by Woodbury and Ludwig [2] and confirmed, among others, by DLTS [97, 129] and Hall effect measurements [102], both combined with EPR

$$Cr_i^{0/+} \quad \text{at} \quad E_c-0.22\,\text{eV}. \tag{29}$$

The existence of a Cr_i^{++} charge state and thus a second donor level (above $E_v+0.05$ eV) is questionable (Sect. 1.2). Hall effect measurements of Kunio et al. [132] and similarly Zolotukhin et al. [23] were explained by a second donor level in Si:Cr near $E_v+0.12$ eV in contradiction to similar experiments of Feichtinger et al. [102], who combined his Hall effect measurements with EPR. That level found near $E_v+0.12$ eV might be due to not identified FeB pairs (Sect. 4.1.5).

Interstitial Cr forms donor-acceptor pairs with substitutional B [1, 2]. These pairs produce a donor level as determined by DLTS [97] and confirmed by combination of DLTS, photo-luminescence and EPR [129]:

$$(Cr_iB_s)^{0/+} \quad \text{at} \quad E_v+0.28\,\text{eV}. \tag{30}$$

In this case room temperature diffusion of interstitial Cr, pair formation and dissociation can be observed looking at these energy levels, the EPR spectra or the characteristic photo-luminescence emission of (CrB) pairs [129].

4.1.4. Si: Mn. Interstitial Mn in silicon has been observed by EPR in four charge states: Mn_i^-, Mn_i^0, Mn_i^+, and Mn_i^{++} [1] (Fig. 1). Recently corresponding energy levels could be determined by DLTS [97] and DLTS with TSCA measurements [128]

$$Mn_i^{-/0} \quad \text{at} \quad E_c-0.11\,\text{eV}, \tag{31}$$

$$Mn_i^{0/+} \quad \text{at} \quad E_c-0.42\,\text{eV}, \tag{32}$$

$$Mn_i^{+/++} \quad \text{at} \quad E_v+0.25\,\text{eV}. \tag{33}$$

These values are corrected for the temperature dependence of the majority carrier capture cross section, which influences the evaluation of energy level by DLTS. Lemke [128] observed room temperature instability of the two donor levels in accordance with the assignment to interstitial Mn. He could not detect the quite shallow acceptor level in the temperature range of his measurements.

In *p*-Si the growth of a new level at $E_c-0.55$ eV during decay of the Mn_i levels was explained by (Mn_iB_s) pair formation [128], a defect which indeed is found by EPR as $(MnB)^+$ [1]. Therefore, this level at $E_c-0.55$ eV might correspond to $(Mn_iB_s)^{0/+}$ but further correlation with EPR is necessary.

4.1.5. Si:Fe. Iron is the most intensively investigated 3*d* impurity in silicon [6–8, 20, 39, 64, 80–85, 88, 89, 130, 131, 133–135]. This is partly due to its frequent uncontrolled presence after any heat treatment of silicon. It is easy to keep iron atoms in interstitial sites during quenching. For several years "thermal defects" were investigated in quenched silicon which we know consist of interstitial iron ([7, 89] and references therein).

The EPR spectra of interstitial iron in silicon (Fe_i^0 and Fe_i^+) have been identified by Ludwig and Woodbury [1] (Fig. 1). The corresponding donor level $Fe_i^{0/+}$ near $E_v+0.4$ eV has been found Collins and Carlson [64]. Combination of EPR and DLTS [133], and EPR and Hall effect measurements [130] confirmed this identification. The concentration of this donor level [6] correlated well with the Fe_i^0 solubility curve obtained by EPR [8]. DLTS measurements frequently locate this level near $E_v+0.45$ eV [6, 83, 133] because of neglection of the temperature dependence of the hole capture cross section. Including this correction, the generally accepted value is now [84, 85, 97]

$$Fe_i^{0/+} \quad \text{at} \quad E_v+0.385\,\text{eV} \tag{34}$$

in agreement with Hall effect measurements [130].

The existence of an acceptor level $Fe_i^{-/0}$ deeper than the phosphorus donor level can be excluded as the EPR spectrum of P_s^0 in *n*-Si is not changed in intensity by the in-diffusion of a comparable Fe concentration [79]. Moreover, room temperature resistivity of *n*-Si is not affected by the presence of interstitial iron [80].

In *p*-type silicon pairing of interstitial iron atoms with shallow acceptors is observed (Sect. 2.3). The existence of donor levels of these pairs can be inferred from EPR (Sect. 1.2). They have been determined by DLTS [6, 85] and Hall effect measurements [131]

$$(FeB)^{0/+} \quad \text{at} \quad E_v+0.105\,\text{eV}, \tag{35}$$

$$(FeAl)^{0/+} \quad \text{at} \quad E_v+0.21\,\text{eV}\ [136]. \tag{36}$$

For (FeGa) recently a donor level has been detected (DLTS) at $E_v+0.24$ eV [85] in agreement with the general trend of deeper pair states for deeper acceptors.

An acceptor level of (FeB) pairs in the upper half of the band gap has been frequently discussed [6, 64, 88, 134]. The energetic position of this level, however, is not yet clear: Hall effect measurements of Collins and Carlson [64] ascribe an acceptor at $E_c-0.55$ eV to FeB pairs (the well-known Au acceptor level has the same ionization energy [5], TSCA experiments yield an acceptor level at $E_c-0.23$ eV [84] the formation and annealing kinetics of which is compatible with FeB pairs. This situation may only be clarified in the future by correlation of electrical measurements with EPR, at best using the same samples.

The nature of a variety of further levels found in iron doped silicon, [135], is not at all clear. They might be due to other pairs and complexes of iron or uncontrolled impurities diffused into silicon during heat treatment. Some of these, like a Fe_4 cluster in annealed and a (Fe+V) pair in electron irradiated, Fe doped silicon, have been recently identified by Muller et al. [20] using EPR. Thus in the future further assignments of levels to specific defects might be achieved.

4.1.6. Si:Co. Cobalt-doped silicon exhibits various deep levels [5, 126]. Microscopic models for the defect configurations are still lacking. No EPR results for Co-related centers have been published. Searches for Co-induced defects by DLTS, attempted by Graff and Pieper [97] were futile although these authors succeeded in detecting many other deep levels produced by 3*d* transition metals. The diffusivity of Co in Si resembles those of Cu or Ni. Therefore, presumably highly mobile Co_i vanishes upon quenching. Precipitation seems likely, similar to Si:Ni or Si:Cu (Sect. 2.3). Mössbauer data by Bergholz [24] support this notion: various Co-related spectral features were interpreted as due to precipitated and possibly substitutional ^{57}Co formed during quenching. No firm conclusions on energy levels in Si:Co are thus possible at present.

4.1.7. Si:Ni. Interstitial Ni supposedly diffuses in a positive charge state at elevated temperatures (Sect. 3.4.3); proof is still lacking. The high diffusivity favours precipitation upon quenching. Interstial Ni_i^+ identified by EPR [1] appears to be in a distorted site, possibly an impurity complex. The EPR data may be correlated with a level at $E_v+0.15$ eV found by DLTS [97], because of comparable defect concentrations which do not depend on diffusion temperature (Sect. 1.2). The DLTS and EPR data seem to be unreconcilable with undistorted interstitial Ni which can be expected to be very unstable at room temperature.

Yoshida et al. [52, 62, 63] described a Ni-related acceptor at $E_c-0.41$ eV produced by merely a small fraction of the total Ni content. Dissociative diffusion (Sect. 2.3) was assumed to explain the diffusion of this presumed substitutional Ni. Microscopic evidence, however, is absent. The solubility of this species obeys [62]

$$x=\exp(7.6-3.1\,[\text{eV}]/kT). \tag{37}$$

The parameters conform to those of Cr, Mn, Fe or Co (Table 2) which suggests complexing of Ni to any of this metals to be involved.

No definite energy levels nor defect configurations for Si:Ni are thus as yet available.

4.1.8. Si:Cu. Cu is the fastest diffusing element in Si (Fig. 2). The diffusion is enhanced by application of an electric field [121], indicating diffusion as Cu_i^+ in agreement with the solubility results (Sect. 3.4.3). However, no donor level of Cu_i has been identified. A pronounced room temperature instability is expected for this defect. Interstitial Cu, as Co_i and Ni_i, vanishes during quenching, partly into precipitates [24, 52, 74, 75], so that in this case, too, no energy level can be established.

4.1.9. Summarizing Discussion. The observed differences in electrical activity of transition metal contaminations in silicon solar cells [123–125] can be qualitatively understood now, considering their stability during cooling and at room temperature: the slowly diffusing Ti and V stay in a great fraction in electrical active (interstitial?) sites after crystal growth. Subsequently they can act as recombination centers. The multiplicity of their charge states supports this killer action but is not decisive as Mn with the same number of charge states is a much less deleterious element. The fastest diffusing Cu_i and Ni_i precipitate even during rapid quenching so that the number of recombination centers stays small despite high total Ni or Cu concentration. The other 3*d* metals in silicon show mean efficiency as lifetime killers corresponding to their intermediate diffusivities.

The energy levels identified for interstitial 3*d* metals in silicon (Table 3 and Fig. 15) show for all these elements the existence of a donor level of the type $M_i^{0/+}$. Generally, the donor level increases in energy with decreasing atomic number. Going from Cr to V, however, a distinct step appears. That decrease from $Cr_i^{0/+}$ to $V_i^{0/+}$ might be due to the effect of a half filled 3*d* shell. V_i^0 takes the $3d^5$ configuration in Si so that adding a fifth electron to V_i^+ ($3d^4$) might be energetically favourable. This feature may provide a critical check for theoretical calculations of 3*d* metal energy levels in silicon. The stability of the $3d^5$ configuration could as well be responsible for the absence of a second donor level $Cr_i^{+/++}$ ($3d^5/3d^4$) found for Mn_i and V_i.

The effect of hydrostatic pressure on the $Fe_i^{0/+}$, $V_i^{+/++}$, $Ti_i^{+/++}$, and $Mn_i^{+/++}$ levels as well as on those of pairs of interstitial Fe with shallow acceptors (B, Al, Ga) has been recently investigated by Wünstel et al. [137]. They found pressure coefficients corresponding to a shift towards the valence band for $Ti_i^{+/++}$, $V_i^{+/++}$, and $Fe_i^{0/+}$ (increasing in this order) and a shift towards the conduction band for $Mn_i^{+/++}$. So all these levels indeed proved to be "deep" as they behave different from the adjacent band. The pressure coefficients of the pair levels are similar to the compression of the band gap indicating a more shallow character of these states, as expected.

A simple model of pressure induced increasing hybridization of the impurity wavefunction with the host predicts a shift towards the conduction band, as observed for chalcogen donors in Si [137]. Yet the opposite is observed for Ti_i, V_i, and Fe_i, so that a strong intra-atomic Coulomb repulsion overcompensating the hybridization effect was discussed in [137]. The conflicting result obtained for $Mn_i^{+/++}$ might be connected with the $3d^5$ configuration of Mn_i^{++}. The level $Cr_i^{0/+}$ with the same electron configurations (Table 3) is thus expected to show a pressure coefficient similar to $Mn_i^{+/++}$.

4.2. Theoretical Approaches

The energy levels of shallow states in semiconductors can be well understood by means of an effective mass theory developed by Kohn and Luttinger (see [138]). This model treats the ionization of substitutional atoms of similar size to host atoms as hydrogenic problem in a medium with a large dielectric constant ε (~ 10) and with carriers of a small effective mass $m^*(\sim 10^{-2} m_0)$, resulting in ionization energies scaled down from the hydrogenic values by $m^*/m_0\varepsilon^2 \sim 10^{-3} - 10^{-4}$. Further refinements of this approach take into account the chemical identity of the impurity ("chemical shift") and corrections to the Coulomb potential close to the impurity ("central cell corrections"). Thus it is possible to describe the number and sequence of levels and energies of excited states. Energy levels, however, are not satisfactorily predicted. For these, better results are achieved by introduction of more realistic impurity potentials, [139].

Effective mass type theories are inappropriate to describe deep impurity states like those introduced by transition metal ions in silicon. This is caused by the localized nature of deep states in contrast to the extended wavefunctions of shallow impurities determined by the long-range Coulomb potential.

For deep level defects in semiconductors two basically different approaches are successfully used, *pertubative and cluster calculations.* In the first case the impurity is treated as a localized pertubation of the perfect solid which can be described in a self-consistent Green's function formalism. Whereas this technique has been applied already to various structural lattice defects in semiconductors, [140, 141], calculations on interstitial transition metals in silicon have not yet been finished with this promising method.

Cluster calculations for defects in semiconductors use techniques developed in quantum chemistry to calculate the electronic structure of "molecules" of a number of silicon atoms, containing the defect at the center. The cluster surface dangling bonds are usually

saturated by means of hydrogen atoms. The simplest kind of cluster calculations, extended Hückel theory, was first employed by Messmer and Watkins for the study of deep levels in semiconductors [142]. It may help to decide the question what defect configuration is the most stable but is hardly useful for calculations of energy levels.

Recently the first successful cluster calculation of the electronic structure and energy levels of interstitial 3*d* metals in silicon has been carried out by De Leo et al. [13–15], using Slater's self-consistent scattered wave X_α cluster method [143–145]. Previously this approach had been applied to substitutional transition metals in silicon [12], for which, however, no reliable experimental data are available.

The approximation used in this method is to draw a sphere around each atom of the cluster (Si and H, respectively) and to spherically average the potential within each sphere. The potential in the interatomic region is taken as constant, as well that outside the cluster. The eigenvalue problem can be solved by means of scattering methods [144].

Energy levels were estimated by Slater's transition state method [145], which is the self-consistent calculation of the single particle level with half an electron in the initial state and half an electron in the final state (corresponding to valence or conduction band).

Using a $Si_{10}H_{16}$ cluster with one of the 3*d* elements Cr, Mn, Fe, Co or Ni at the interstitial position in the center, De Leo et al. [13–15] confirmed the assumptions of the Ludwig and Woodbury model [1] (Sect. 1.2 and Fig. 1):

(*i*) For the interstitial T-metal, in fact, no states corresponding to 4*s* electrons are found so that these electrons are included in the 3*d* states.

(*ii*) The crystal field splitting of the 3*d* states results in lowering the t_2 state with respect to the *e* state.

(*iii*) A spin unrestricted calculation, which only converged after lowering the bonding distance of the Si–H terminators, proved the splitting between states of opposite spin to be larger than the crystal field splitting so that Hund's rule is fulfilled.

The energy levels, computed including many-electron effects, are included in Fig. 15. The increasing (0/+) donor level between Fe and Cr is reproduced well, even better the separation of the $Mn_i^{-/0}$ and $Mn_i^{0/+}$ levels amounting to 0.31 eV. However, the step from Cr to V is not in accordance with this model. Moreover, V_i is predicted to be unstable in the V_i^0 state and thus even more in the V_i^- state, and Fe_i should be an acceptor. Whereas the first question still might be debated as long as V_i^0 or V_i^- have not yet been observed by EPR, an acceptor level of Fe_i must be – if at all existing in the gap – very close to the conduction band, as discussed in Sect. 4.1.5.

Thus these first calculations are promising but do not yet explain all experimental evidence. Definitely a great success is the verification of the Ludwig and Woodbury model. The remaining inconsistencies with experiment might be resolvable in the future. Most valuable would be predictions for those elements for which reliable experimental results are not yet available, especially Co_i, Ni_i, and Cu_i.

Finally it can be expected that in the near future the results of other calculations, including the use of the Green's function formalism, will be available.

5. Summary

This review allows to draw the following conclusions:

– 3*d* transition elements diffuse predominantly as interstitials in Si with an activation energy of diffusion near 0.75 eV.

– They stay in interstitial sites at high temperature in thermal equilibrium.

– The liquidus curves of the Si:Ti to Si:Ni melts can be described by the same parameters indicating comparable interaction energies of silicon with all these 3*d* transition metals.

– The solid solubilities allow a distinction into two groups according to the formation enthalpies in silicon:

"3*dI*" elements: (Ti, V?), Cr, Mn, Fe, Co with:

$\Delta H^s \cong 2.1$ eV

"3*dII*" elements: Ni, Cu yielding:

$\Delta H^s \cong 1.5$ eV;

a possible explanation might be:

3*dI* atoms diffuse as neutral interstitials, and
3*dII* atoms as positively charged interstitials.

– (Ti?), V, Cr, Mn, and Fe can be quenched in interstitial sites of tetrahedral symmetry,
Co, Ni, and Cu vanish out of the interstitial solutions during quenching.

– Energy levels for the interstitial species and various pairs have been established, based mainly on combinations of different experimental methods with EPR results.

– Substitutional 3*d* metals in silicon are rather exotic species, produced under non-equilibrium conditions like irradiation. Their energy levels cannot be established at present.

– The great differences in the degradation effect of 3*d*-type impurities in silicon solar cells appear to be due to the different thermal stability of these transition elements.

Further properties of transition metal defects in silicon, especially optical properties such as photoluminescence, are just starting to be related to specific defect configurations. Information on the diffusivity, solubility, thermal stability and electrical properties of 3*d* metals in silicon presented in this paper might provide substantial support for future identifications.

Acknowledgements. The author is indebted to Professor H. Alexander for encouragement and many stimulating discussions in the course of this work. The cooperation with Prof. W. Herr, Dr. U. Herpers, Dr. H. G. Riotte, and especially Dr. N. Wiehl concerning the neutron activation analyses is gratefully acknowledged. For interesting discussions and valuable hints special thanks are due to Dr. W. Bergholz, Dr. G. Borchardt, Prof. J. W. Corbett, Dr. H. Feichtinger, Prof. W. Frank, Dr. K. Graff, Prof. H. J. Queisser, Prof. W. Schröter, and Prof. G. D. Watkins. Technical assistance of Mrs. R. Küpper, Mrs. G. Schemann, and Mrs. E. Simon was very helpful. Dr. W. Zulehner, Wacker-Chemitronic, supplied specially doped silicon crystals. The "Deutsche Forschungsgemeinschaft" gave financial support and provided equipment.

References

1. G.W. Ludwig, H.H. Woodbury: Solid State Phys. **13**, 223 (1962)
2. H.H. Woodbury, G.W. Ludwig: Phys. Rev. **117**, 102 (1960)
3. F.A. Trumbore: Bell. Syst. Tech. J. **39**, 205 (1960)
4. K.V. Ravi: *Imperfections and Impurities in Semiconductor Silicon* (Wiley, New York 1981)
5. J.W. Chen, A.G. Milnes: Annu. Rev. Mater. Sci. **10**, 157 (1980)
6. K. Graff, H. Pieper: J. Electrochem. Soc. **128**, 669 (1981)
7. E. Weber, H.G. Riotte: Appl. Phys. Lett. **33**, 433 (1978)
8. E. Weber, H.G. Riotte: J. Appl. Phys. **51**, 1484 (1980)
9. N. Wiehl, U. Herpers, E. Weber: In *Nuclear Physics Methods in Materials Research*, ed. by K. Bethge, H. Baumann, H. Jex, and F. Rauch (Vieweg, Braunschweig 1980) p. 334
10. N. Wiehl, U. Herpers, E. Weber: J. Radioanal. Chem. **72**, 69 (1982)
11. E.R. Weber, N. Wiehl: To be published
12. L.A. Hemstreet: Phys. Rev. B**15**, 834 (1977)
13. G.G. DeLeo, G.D. Watkins, W.B. Fowler: Phys. Rev. B**23**, 1851 (1981)
14. G.G. DeLeo, G.D. Watkins, W.B. Fowler: Phys. Rev. B**25**, 4962 (1982)
15. G.G. DeLeo, G.D. Watkins, W.B. Fowler: Phys. Rev. B**25**, 4972 (1982)
16. B.I. Boltaks: *Diffusion in Semiconductors* (Infosearch, London 1963)
17. B.L. Sharma: *Diffusion in Semiconductors* (Trans. Tech. Publications, Clausthal-Zellerfeld 1970)
18. T. Chang, A.H. Kahn: NBS Special Publication **260–259** (1978)
19. G.D. Watkins: In *Point Defects in Solids*, ed. by J.H. Crawford, Jr. and L.M. Slifkin (Plenum Press, New York, London 1975) p. 333
20. S.H. Muller, G.M. Tuynman, E.G. Sieverts, C.A.J. Ammerlaan: Phys. Rev. B**25**, 25 (1982)
21. G.W. Ludwig, H.H. Woodbury, R.O. Carlson: Phys. Chem. Solids **8**, 490 (1959)
22. A.A. Bugai, V.S. Vikhnin, V.E. Kustov, V.M. Maksimenko, B.K. Krulikovskii: Zh. Eksp. Teor. Fiz. **74**, 2250 (1978) [Sov. Phys. JETP **47**, 1170 (1978)]
23. A.A. Zolotukhin, L.S. Milevskii: Fiz. Tverd. Tela **13**, 1906 (1971) [Sov. Phys. Solid State **13**, 1598 (1972)]
24. W. Bergholz: J. Phys. D**14**, 1099 (1981)
25. E. Weber, N. Wiehl: Verhandl. DPG (VI) **15**, 223 (1980)
26. D.F. Daly: J. Appl. Phys. **42**, 864 (1971)
27. Y.H. Lee, J.W. Corbett: Phys. Rev. B**8**, 2810 (1973)
28. E.G. Sieverts: Phys. Status Solidi (1982, in press)
29. H.G. Riotte, U. Herpers, E. Weber: Radiochim. Acta **27**, 209 (1980)
30. C.T. Sah, W.W. Chan, H.S. Fu, J.W. Walker: Appl. Phys. Lett. **20**, 193 (1972)
31. D.V. Lang: J. Appl. Phys. **45**, 3032 (1974)
32. G.L. Miller, D.V. Lang, L.C. Kimerling: Annu. Rev. Mater. Sci. **7**, 377 (1977)
    D.V. Lang: In *Thermally Stimulated Relaxation in Solids*, ed. by P. Bräunlich, Topics Appl. Phys. **37** (Springer, Berlin, Heidelberg, New York 1979)
33. H.G. Grimmeiss: Annu. Rev. Mater. Sci. **7**, 341 (1977)
34. S.M. Hu: In *Atomic Diffusion in Semiconductors*, ed. by D. Shaw (Plenum Press, New York 1973) p. 217
35. V.P. Boldyrev, I.I. Pokrovskii, S.G. Romanovskaya, A.V. Tkach, I.E. Shimanovich: Fiz. Tekh. Poluprovodn. **11**, 1199 (1977) [Sov. Phys. Semicond. **11**, 709 (1977)]
36. E. Ohta, M. Sakata: Solid-State Electron. **23**, 759 (1980)
37. N.T. Bendik, V.S. Garnyk, L.S. Milevskii: Fiz. Tverd. Tela **12**, 190 (1970) [Sov. Phys. Solid State **12**, 150 (1970)]
38. M.K. Bakhadyrkhanov, B.I. Boltaks, G.S. Kulikov: Fiz. Tverd. Tela **14**, 1671 (1972) [Sov. Phys. Solid State **14**, 1441 (1972)]
39. J.D. Struthers: J. Appl. Phys. **27**, 1560 (1956)
40. L.C. Kimerling: In *Defects in Semiconductors*, ed. by J. Narayan and T.Y. Tan (North-Holland, New York, Oxford 1981) p. 85
41. M.K. Bakhadyrkhanov, B.I. Boltaks, G.S. Kulikov: Fiz. Tverd. Tela **12**, 181 (1970) [Sov. Phys. Solid State **12**, 144 (1970)]
42. M.K. Bakhadyrkhanov, S. Zainabidinov, A. Khamidov: Fiz. Tekh. Poluprovodn. **14**, 412 (1980) [Sov. Phys. Semicond. **14**, 243 (1980)]
43. R.N. Hall, J.H. Racette: J. Appl. Phys. **35**, 379 (1964)
44. M.K. Bakhadyrkhanov, B.I. Boltaks, G.S. Kulikov, E.M. Pedyash: Fiz. Tekh. Poluprovodn. **4**, 873 (1970) [Sov. Phys. Semicond. **4**, 739 (1970)]
45. E.M. Pell: Phys. Rev. **119**, 1222 (1960)
46. M. Okamura: Jpn. J. Appl. Phys. **8**, 1440 (1969)
47. C.S. Fuller, J.A. Ditzenberger: J. Appl. Phys. **27**, 544 (1956)
48. H.J. Mayer, H. Mehrer, K. Maier: In *Radiation Effects in Semiconductors 1976*, ed. by N.B. Urli and J.W. Corbett (Inst. of Physics, Bristol, London 1977) Conf. Ser. **31**, p. 186
49. H. Kitagawa, K. Hashimoto: Jpn. J. Appl. Phys. **16**, 173 (1977)
50. H.P. Bonzel: Phys. Status Solidi **20**, 493 (1967)
51. J.H. Aalberts, M.L. Verheijke: Appl. Phys. Lett. **1**, 19 (1962)
52. M. Yoshida, K. Furusho: Jpn. J. Appl. Phys. **3**, 521 (1964)
53. A.F.W. Willoughby: Rep. Prog. Phys. **41**, 1665 (1978)
54. U. Gösele, W. Frank: In *Defects in Semiconductors*, ed. by J. Narayan and T.Y. Tan (North-Holland, New York, Oxford 1981) p. 55
55. J.A. Van Vechten, C.D. Thurmond: Phys. Rev. B**14**, 3551 (1976)
56. A. Seeger, W. Frank, U. Gösele: In *Defects and Radiation Effects in Semiconductors 1978*, ed. by J.H. Albany (Inst. of Physics, Bristol, London 1979) Conf. Ser. **46**, p. 148
57. W. Frank, A. Seeger, U. Gösele: In *Defects in Semiconductors*, ed. by J. Narayan and T.Y. Tan (North-Holland, New York, Bristol 1981) p. 31
58. J.C. Brice: *The Growth of Crystals from the Melt* (North-Holland, Amsterdam 1965)

59. Y.H. Lee, R.L. Kleinhenz, J.W. Corbett: In *Defects and Radiation Effects in Semiconductors 1978*, ed. by J.H. Albany (Inst. of Physics, Bristol, London 1979) Conf. Ser. **46**, p. 521
60. Quenching experiments from 1250 °C using phosphorus doped silicon failed to detect by EPR Si-E centers (P_s+V), the dominant defect in irradiated *n*-Si. The detection limit was lower than $10^{11}\,cm^{-3}$ [79]
61. M. Lannoo, J.C. Bourgoin: Solid State Commun. **32**, 913 (1973)
62. M. Yoshida, K. Saito: Jpn. J. Appl. Phys. **6**, 573 (1967)
63. H. Kitagawa, K. Hashimoto, M. Yoshida: Jpn. J. Appl. Phys. **21**, 276 (1982)
64. C.B. Collins, R.O. Carlson: Phys. Rev. **108**, 1409 (1957)
65. F.C. Frank, D. Turnbull: Phys. Rev. **104**, 617 (1956)
66. F.A. Huntley, A.F.W. Willoughby: J. Electrochem. Soc. **120**, 414 (1973)
67. D.V. Lang, H.G. Grimmeiss, E. Meijer, M. Jaros: Phys. Rev. B**22**, 3917 (1980)
68. M. Höhne: Phys. Status Solidi B**99**, 651 (1980)
69. R.L. Kleinhenz, Y.H. Lee, J.W. Corbett, E.G. Sieverts, S.H. Muller, C.A.J. Ammerlaan: Phys. Status Solidi B**108**, 363 (1981)
70. E.R. Weber, N. Wiehl, G. Borchardt, S.D. Brotherton: To be published
71. V.A. Uskov: Izv. Akad. Nauk SSR, Neorg. Mater. **11**, 991 (1975) [Inorg. Mater. (USSR) **11**, 848 (1975)]
72. Y. Yamaguchi, M. Yoshida, H. Aoki: Jpn. J. Appl. Phys. **2**, 714 (1963)
73. M. Stoijć, V. Spirić, D. Kostoski: Fizika (Zagreb) **12**, Suppl. 1, 70 (1980)
74. W.C. Dash: Phys. Rev. **98**, 1536 (1955)
75. Y. Chikaura, K. Kishimoto: Jpn. J. Appl. Phys. **19**, L5 (1980)
76. M.K. Bakhadyrkhanov, S. Zainoabidinov: Fiz. Tekh. Poluprovodn. **12**, 683 (1978) [Sov. Phys. Semicond. **12**, 398 (1978)]
77. A.G. Cullis, L.E. Katz: Philos. Mag. **30**, 1419 (1974)
78. A. Goetzberger, W. Shockley: J. Appl. Phys. **31**, 1821 (1960)
79. E.R. Weber: Unpublished
80. A.A. Lebedev, B.M. Urunbaev: Fiz. Tekh. Poluprovodn. **15**, 612 (1981) [Sov. Phys. Semicond. **15**, 350 (1981)]
81. E. Weber: Crystal Res. Techn. **16**, 209 (1981)
82. E. Weber: Verhandlg. DPG (VI) **16**, 250 (1981)
83. L.C. Kimerling, J.L. Benton, J.J. Rubin: In *Defects and Radiation Effects in Semiconductors 1980*, ed. by R.R. Hasiguti (Inst. of Physics, Bristol, London 1981) Conf. Ser. **59**, p. 217
84. H. Lemke: Phys. Status Solidi A**64**, 215 (1981)
85. K. Wünstel, P. Wagner: Appl. Phys. A**27**, 207 (1982)
86. H. Reiss, C.S. Fuller, F.J. Morin: Bell Syst. Tech. J. **35**, 535 (1956)
87. L.C. Kimerling: Solid-State Electron. **21**, 1391 (1978)
88. W.H. Shepherd, J.A. Turner: J. Phys. Chem. Sol. **23**, 1697 (1962)
89. Y.H. Lee, R.L. Kleinhenz, J.W. Corbett: Appl. Phys. Lett. **31**, 142 (1977)
90. G.W. Ludwig, H.H. Woodbury: Proc. Intern. Conf. on Semicond. Physics, Prague (1960) p. 596
91. R.A. Swalin: J. Phys. Chem. Sol. **23**, 153 (1962)
92. L. Pauling: *The Nature of the Chemical Bond* (Cornell Press, Ithaca 1940)
93. K. Weiser: Phys. Rev. **126**, 1427 (1962)
94. F.D.M. Haldane, P.W. Anderson: Phys. Rev. B**13**, 2553 (1976)
95. A. Zunger, U. Lindefelt: To be published
96. J.W. Chen, A.G. Milnes, A. Rohatgi: Solid-State Electron. **22**, 801 (1979)
97. K. Graff, H. Pieper: In *Semiconductor Silicon 1981*, ed. by H.R. Huff, R.J. Kriegler, and Y. Takeishi (The Electrochem. Soc., Pennington 1981) p. 331
98. H. Kitagawa, K. Hashimoto: Jpn. J. Appl. Phys. **16**, 857 (1977)
99. R.C. Dorward, J.S. Kirkaldy: Trans. Metall. Soc. AIME **242**, 2055 (1968)
100. C.D. Thurmond, J.D. Struthers: J. Phys. Chem. **57**, 831 (1953)
101. W. Würker, K. Roy, J. Hesse: Mater. Res. Bull. **9**, 971 (1974)
102. H. Feichtinger, R. Czaputa: Appl. Phys. Lett. **39**, 706 (1981)
103. M. Hansen, K. Anderko: *Constitution of Binary Alloys* (McGraw-Hill, New York 1958)
104. F.A. Shunk: *Constitution of Binary Alloys*, 2nd Suppl. (McGraw-Hill, New York 1969)
105. K.N. Tu, J.W. Mayer: In *Thin Films – Interdiffusion and Reactions*, ed. by J.M. Poate, K.N. Tu, and J.W. Mayer (Wiley, New York 1978) p. 359
106. G. Ottaviani, K.N. Tu, J.W. Mayer: Phys. Rev. B**24**, 3554 (1981)
107. F.A. Veer, B.H. Kolster, W.G. Burgers: Trans. Metall. Soc. AIME **242**, 689 (1968)
108. O. Kubaschewski, E.L.L. Evans, C.B. Alcock: *Metallurgical Thermochemistry* (Pergamon Press, Oxford 1967)
109. For Si:Cu the validity of this assumption (i.e. $\gamma_2^1=1$) has been proved [99], resulting only in a minor correction of $\mathcal{K}$ due to the introduction of $\gamma_2^1 \neq 1$
110. R.C. Weast (ed.): *Handbook of Chemistry and Physics*, 56th ed. (CRC Press, Cleveland 1975)
111. C.D. Thurmond, M. Kowalchik: Bell Syst. Tech. J. **39**, 169 (1960)
112. A.M. Alper: *Phase Diagrams* (Academic Press, New York, London 1970)
113. S. Fischler: J. Appl. Phys. **33**, 1615 (1962)
114. H. Statz: J. Phys. Chem. Sol. **24**, 669 (1963)
115. K. Lehovec: J. Phys. Chem. Sol. **23**, 695 (1962)
116. O. Kubaschewski, J.A. Catterall: *Thermochemical Data of Alloys* (Pergamon Press, Oxford 1956)
117. W.T. Stacy, D.F. Allison, T.-C. Wu: In *Semiconductor Silicon 1981*, ed. by H.R. Huff, R.J. Kriegler, and Y. Takeishi (The Electrochemical Society, Pennington 1981) p. 344
118. T.M. Buck, J.M. Poate, K.A. Pickar, C.M. Hsieh: Surf. Sci. **35**, 362 (1973)
119. J.A. Van Vechten: In *Handbook on Semiconductors*, Vol. 3, ed. by S.P. Keller (North-Holland, New York, Oxford 1980) p. 1
120. C.S. Fuller, J.C. Severins: Phys. Rev. **96**, 21 (1954)
121. C.J. Gallagher: J. Phys. Chem. Solids **3**, 82 (1957)
122. K. Weiser: J. Phys. Chem. Solids **17**, 149 (1960)
123. R.H. Hopkins, R.G. Seidensticker, J.R. Davies, P. Rai-Choudhury, P.D. Blais, J.R. McCormick: J. Cryst. Growth **42**, 493 (1977)
124. A. Rohatgi, J.R. Davies, R.H. Hopkins, P. Rai-Choudhury, P.G. McMullin, J.R. McCormick: Solid-State Electron. **23**, 415 (1980)
125. J.R. Davies, A. Rohatgi, R.H. Hopkins, P.D. Blais, P. Rai-Choudhury, J.R. McCormick, H.C. Mollenkopf: IEEE Trans. ED-**27**, 677 (1980)
126. A.G. Milnes: *Deep Impurities in Semiconductors* (Wiley, New York 1973)
127. A.M. Salama, L.J. Cheng: J. Electrochem. Soc. **127**, 1164 (1980)
128. H. Lemke: Phys. Status Solidi A**64**, 549 (1981)
129. H. Conzelmann, K. Graff, E.R. Weber: To be published
130. H. Feichtinger, J. Waltl, A. Gschwandtner: Solid State Commun. **27**, 867 (1978)
131. H. Feichtinger: Acta Phys. Austr. **51**, 161 (1979)
132. T. Kunio, T. Nishino, E. Ohta, M. Sahata: Solid-State Electron. **24**, 1087 (1981)
133. J.D. Gerson, L.J. Cheng, J.W. Corbett: J. Appl. Phys. **48**, 4821 (1977)

134. M.A. Abdugafurova, L.M. Kapitonova, L.S. Kostina, A.A. Lebedev, Sh. Makhkamov: Fiz. Tekh. Poluprovodn. **9**, 685 (1975) [Sov. Phys. Semicond. **9**, 450 (1975)]
135. K. Wünstel, P. Wagner: Solid State Commun. **40**, 797 (1981)
136. Graff et al. [6] ascribe the $E_v+0.21$ eV level to an (FeAl) acceptor and $E_v+0.13$ eV to the (FeAl) donor; however, as pointed out by Wünstel and Wagner [85] the lower level has to be due to some other complex and, in accordance with Feichtinger [131] the upper level corresponds to the $(FeAl)^{0/+}$ donor, [97]
137. K. Wünstel, O. Kumagai, P. Wagner, W. Jantsch: Appl. Phys. A**27**, 251 (1982)
138. W. Kohn: Solid State Phys. **5**, 257 (1957)
139. S.T. Pantelides: Rev. Mod. Phys. **50**, 797 (1978)
140. G.A. Baraff, M. Schlüter: Phys. Rev. Lett. **41**, 892 (1978)
141. J. Bernholc, S.T. Pantelides: Phys. Rev. B**18**, 1780 (1978)
142. R.P. Messmer, G.D. Watkins: Phys. Rev. B**7**, 2568 (1973)
143. K.H. Johnson, F.C. Smith: Phys. Rev. B**5**, 831 (1972)
144. J.C. Slater, K.H. Johnson: Phys. Rev. B**5**, 844 (1972)
145. J.C. Slater: *The Self-Consistent Field for Molecules and Solids* (McGraw-Hill, New York 1974)